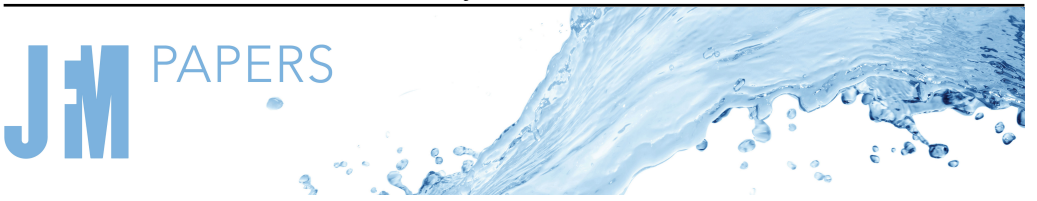
J. Fluid Mech. (2025), *vol.* 1011, A44, doi:10.1017/jfm.2025.323



Constructing turbulence models using the kinetic Fokker–Planck equation

Peng Luan[1,†], **Haoyuan Zhang**[2,3,†] and **Jun Zhang**[1]

[1]School of Aeronautic Science and Engineering, Beihang University, Beijing 100191, PR China

[2]State Key Laboratory of Aerodynamics, Mianyang 621000, PR China

[3]Computational Aerodynamics Institute, China Aerodynamics Research and Development Center, Mianyang 621000, PR China

Corresponding author: Jun Zhang, jun.zhang@buaa.edu.cn

(Received 21 October 2024; revised 10 March 2025; accepted 18 March 2025)

This study presents a novel approach for constructing turbulence models using the kinetic Fokker–Planck equation. By leveraging the inherent similarities between Brownian motion and turbulent dynamics, we formulate a Fokker–Planck equation tailored for turbulence at the hydrodynamic level. In this model, turbulent energy plays a role analogous to temperature in molecular thermodynamics, and the large-scale structures are characterised by a turbulent relaxation time. This model aligns with the framework of Pope's generalised Langevin model, with the first moment recovering the Reynolds-averaged Navier–Stokes (RANS) equations, and the second moment yielding a partially modelled Reynolds stress transport equation. Utilising the Chapman–Enskog expansion, we derive asymptotic solutions for this turbulent Fokker–Planck equation. With an appropriate choice of relaxation time, we obtain a linear eddy viscosity model at first order, and a quadratic Reynolds stress constitutive relationship at second order. Comparative analysis of the coefficients of the quadratic expression with typical nonlinear viscosity models reveals qualitative consistency. To further validate this kinetic-based nonlinear viscosity model, we integrate it as a RANS model within computational fluid dynamics codes, and calculate three typical cases. The results demonstrate that this quadratic eddy viscosity model outperforms the linear model and shows comparability to a cubic model for two-dimensional flows, without the introduction of *ad hoc* parameters in the Reynolds stress constitutive relationship.

Key words: kinetic theory, turbulence modelling

[†] These two authors contributed equally to this work.

© The Author(s), 2025. Published by Cambridge University Press.

https://doi.org/10.1017/jfm.2025.323 Published online by Cambridge University Press

1. Introduction

Turbulence is a highly complex, irregular flow phenomenon that occurs in liquids, gases and plasma, making it ubiquitous in both nature and engineering applications (Pope 2001). Although the numerical integration of the Navier–Stokes (NS) equations is a crucial tool for studying the fundamental mechanisms of turbulent flows, even the most powerful foreseeable computers are unable to perform direct numerical simulations (DNS) for most engineering and environmental flows (Moin & Mahesh 1998). Therefore, significant efforts are devoted to modelling the effects of the small, unresolved scales on the large, resolved ones – an approach known as turbulence modelling (Wilcox 1998).

Since the pioneering work of Reynolds (1895), the Reynolds-averaged NS (RANS) approach has served as a fundamental framework on turbulence modelling. A major challenge in the RANS approach is to express the Reynolds stress in terms of the mean field and its properties, with early efforts relying on eddy viscosity concepts and dimensional scaling (Durbin 2018). This foundation continues today, with linear eddy viscosity models (EVMs) (Launder & Spalding 1983; Spalart & Allmaras 1992; Menter 1997; Wilcox 2008) and nonlinear eddy viscosity models (NLEVMs) (Pope 1975; Speziale 1987; Gatski & Speziale 1993; Craft *et al.* 1996; Wallin & Johansson 2000; Fu *et al.* 2011). Additionally, there have been attempts to go beyond the EVMs to capture complex strain patterns, including anisotropy and history effects (Launder *et al.* 1975; Hanjalić 1994). Despite these advances, a significant gap remains in understanding turbulent fluctuations and their effects on mean flows. As a result, closure modelling often blends analysis, analogy and empiricism, with models sometimes relying on variables that lack clear physical meaning and remaining heavily empirical (Durbin 2018).

In addition to semi-empirical approaches, there have been attempts to derive turbulent models from a theoretical perspective. Notable efforts include the use of Kraichnan's DIA formalism by Yoshizawa (1984), the application of the RNG method by Rubinstein & Barton (1990), and the use of the double expansion method by Yakhot *et al.* (1992), all of which have achieved relatively successful results. Broadly speaking, these models are based on various averaging procedures within the coarse-grained NS description.

The coarse-grained NS approach, incorporating eddy viscosity concepts, has been undeniably successful but suffers from a key limitation: the assumption of scale separation between the mean and fluctuating fields (Monin & Yaglom 2013). While this assumption works well for molecules, it breaks down for fully developed turbulence, where no such clear scale separation exists. Simple estimations reveal that the effective mean free path of eddies (i.e. the Prandtl mixing length) is comparable to the characteristic scales of the mean flow (Wilcox 1998). Hence a theoretical and computational framework capable of addressing the eddy interactions across different scales of motion is required. Notably, kinetic equations such as the Boltzmann equation do not rely on a separation between microscopic and macroscopic scales (Cercignani 1988), making them ideally suited for this purpose. Previous research has demonstrated that the Boltzmann equation is capable of accurately describing turbulent flows (Gallis *et al.* 2017; McMullen *et al.* 2022). As such, it is believed that coarse-grained kinetic equations inherently contain all potential turbulence models, regardless of their nonlinearity and complexity.

Indeed, the connections between turbulence modelling and kinetic theory are profound. The concept of eddy viscosity, along with the analogy between microscopic thermal effects and macroscopic eddy effects, has been a cornerstone of both theoretical and engineering models of turbulence to this day (Wilcox 1998; Pope 2001). This understanding dates back to Lord Kelvin (Thomson 1887), who highlighted the analogy between Maxwell's kinetic theory of gas molecules and eddy transport in turbulence. The well-known Boussinesq approximation (Boussinesq 1870) fully analogises the motions of

https://doi.org/10.1017/jfm.2025.323 Published online by Cambridge University Press

turbulent eddies to the behaviour of molecules in kinetic theory. Prandtl's mixing-length hypothesis (Prandtl 1925) borrows the concept of the molecular mean free path from kinetic theory. Interestingly, Chen *et al.* (2004) quantify the analogy beyond simple eddy viscosity by exploring the relationship between higher-order (nonlinear and non-Newtonian) kinetic theory and higher-order turbulence models. Their findings reveal that turbulence modelling is grounded in kinetic theory more firmly than previously recognised.

Recently, several attempts have been made to study turbulence from the perspective of kinetic theory, often employing a Bhatnagar–Gross–Krook (BGK)-type model as a starting point. For instance, Chen *et al.* (2003) formulated a kinetic theoretical representation of turbulence using a BGK-type model, achieving significant success with the lattice Boltzmann method to simulate complex turbulent flows. Chen *et al.* (2023) further demonstrated this effective BGK-type model for fluid particles can be constructed by averaging the Klimontovich-type kinetic equation. Moreover, Chen *et al.* (2024) showed that the relaxation time in this model can be theoretically estimated for homogeneous, isotropic, and stationary turbulent flow, yielding a turbulent viscosity coefficient that closely agrees with values obtained from existing turbulence modelling approaches. Girimaji (2007) developed a kinetic Boltzmann equation for describing filtered fluid turbulence, applicable to both continuum and non-continuum effects, thereby paving the way for unifying turbulence modelling at both kinetic and continuum levels. Yakhot (2007) explored a coarse-grained kinetic equation by introducing a 'two-level' phase space and integrating out the fast microscopic variables. This coarse-grained kinetic equation serves as the foundation for several turbulence models. Malaspinas & Sagaut (2012) proposed a consistent method for introducing subgrid closures into the BGK equation for large eddy simulations of turbulent flows. They constructed a hierarchy of subgrid-scale terms by employing the Hermite expansion of the velocity distribution function. Succi (2020) presented a closure for the effective relaxation time of the BGK model for turbulence, based on a double-averaging procedure over both kinetic and turbulent fluctuations. Samiee *et al.* (2020) utilised a Lévy-stable distribution to model the equilibrium distribution function in the filtered BGK equation, leading to the proposed fractional-order modelling of subgrid-scale stresses.

As an alternative, this work investigates turbulence from a stochastic modelling perspective, specifically using the Fokker–Planck equation. In kinetic theory, the Fokker–Planck equation can be regarded as an approximation of the Boltzmann equation, and can also be derived independently from the Kramers–Moyal equation (Cercignani 1988). Besides, the Fokker–Planck equation is equivalent to Langevin dynamics, which is computationally efficient (Jenny *et al.* 2010) and effectively describes the Brownian motion of particles (Langevin 1908). Pioneering studies in this area include work by Kirkwood (1946) and Kirkwood *et al.* (1949) on liquids, as well as by Heinz (2003, 2004) on monatomic gases.

In turbulence modelling, the probability density function (PDF) method proposed by Pope (1985) and the filtered density function method proposed by Heinz (2007) demonstrated the Fokker–Planck equation's effectiveness in describing turbulence. Chung (1969) adapted a modified Fokker–Planck equation to govern the distribution functions of fluid particles and, by extension, chemical species. Mishra & Girimaji (2016) applied a generalised set of Langevin equations to generate manufactured turbulence, which replicates the behaviour of physical turbulence rather than modelling it directly. Additionally, recent findings from both experiments and numerical simulations (Chong *et al.* 2020) indicate that the movement of vortices in a rotating turbulent convective flow resembles that of inertial Brownian particles, moving ballistically initially and then

https://doi.org/10.1017/jfm.2025.323 Published online by Cambridge University Press

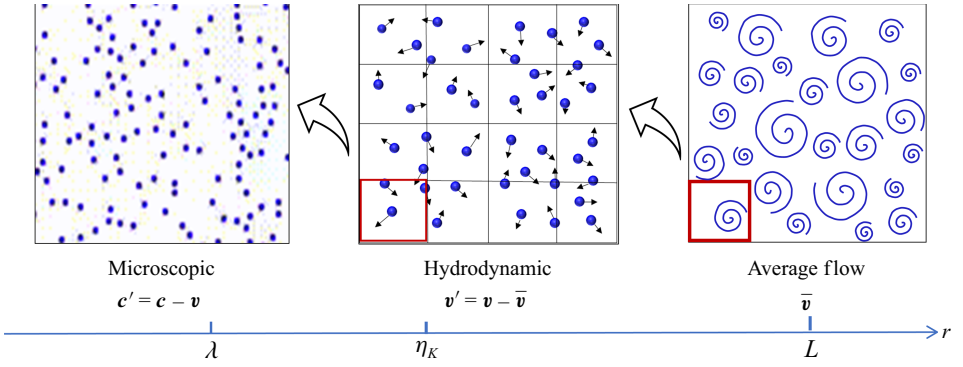


Figure 1. Schematic diagram of scales of length and velocity fields defined in turbulence.

diffusively after a certain critical time. These studies suggest that the Fokker–Planck equation is a promising tool with which to study turbulence.

The aim of this study is to construct turbulence models for RANS using the kinetic Fokker–Planck equation. This procedure is self-consistent and reduces reliance on *ad hoc* parameters, offering a more physically grounded framework for capturing turbulent behaviour. The remainder of the paper is organised as follows. Section 2 presents the turbulence modelling procedure. In § 3, we validate the turbulence models obtained, including comparisons of coefficients with typical NLEVMs and comparisons of computational results with experimental data. Section 4 provides concluding remarks and discussions.

2. Turbulence modelling

2.1. *Turbulence modelling from a kinetic perspective*

The study and simulation of turbulence can be categorised into three distinct levels: the microscopic level, the hydrodynamic level, and the average flow field level. Each of these levels corresponds to a specific characteristic length (Wilcox 1998; Yakhot 2007): the molecular mean free path scale λ, the Kolmogorov length scale $\eta_K \approx LRe^{-3/4}$, Re is the Reynolds number and the macroscopic length scale L, as depicted in figure 1.

At the microscopic level ($r \approx \lambda$), our focus begins with molecules, where the velocity fields emphasise molecular velocities – specifically, the molecules' instantaneous velocities $\boldsymbol{c}$, and their thermal velocities $\boldsymbol{c}'$. The thermal velocity can be determined by $\boldsymbol{c}' = \boldsymbol{c} - \boldsymbol{v}$, where $\boldsymbol{v}$ represents the instantaneous velocity of a fluid particle. At the hydrodynamic level, fluid particles serve as the fundamental elements. Hydrodynamic approximations can be obtained by eliminating small-scale modes from the interval $r \leqslant \eta_K$, resulting in the velocities of fluid particles – specifically, their instantaneous velocities $\boldsymbol{v}$, and their fluctuating velocities $\boldsymbol{v}'$. The fluctuating velocity can be determined by $\boldsymbol{v}' = \boldsymbol{v} - \bar{\boldsymbol{v}}$, where $\bar{\boldsymbol{v}}$ represents the mean velocity at the average flow field level. Subsequently, turbulence models can be derived by averaging over the interval $\eta_K \leqslant r \leqslant L$, focusing solely on mean velocities.

In principle, kinetic equations, such as the Boltzmann equation and its simplified models, can provide a comprehensive description of turbulence at the microscopic level (Gallis *et al.* 2017; McMullen *et al.* 2022). Based on this foundation, there are two fundamental approaches for deriving turbulence models at the average flow field level from kinetic equations (Succi 2020). As depicted in figure 2, the first approach involves

https://doi.org/10.1017/jfm.2025.323 Published online by Cambridge University Press

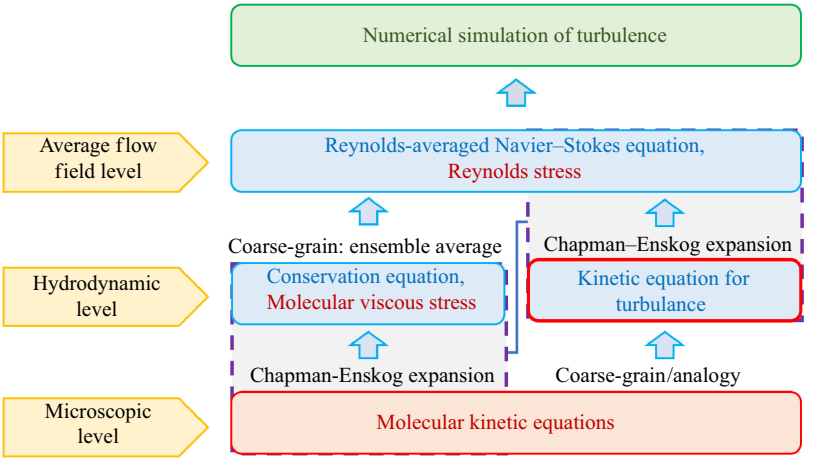


Figure 2. Two basic approaches to coarse-graining the kinetic equations to obtain turbulence models at the average flow field level.

initially projecting out the velocity degrees of freedom from the kinetic equations to derive conservation equations – namely, the mass and momentum conservation equations – at the hydrodynamic level. The appearance of molecular viscous stress makes these equations unclosed. Assuming a weak departure from local equilibrium, we can apply the Chapman–Enskog expansion (Chapman & Cowling 1990) to link the molecular viscous stress with hydrodynamic variables. Truncating this expansion to the first order yields the NS equations. By further coarse-graining the NS equations through ensemble averaging, we can derive the RANS equations with Reynolds stress, which forms the foundation of mainstream turbulence modelling.

The second approach begins by constructing a kinetic equation for turbulence at the hydrodynamic level from the molecular kinetic equations, either through coarse-graining or by analogy. Then by projecting out the velocity degrees of freedom from this kinetic equation, the RANS equations can be derived. To close these equations, the Chapman–Enskog expansion can be used to derive a constitutive relationship between the Reynolds stress and the average flow field variables. This methodology is adopted in the current study.

Symbolically, the first approach (the hydrodynamic approach) can be expressed as

$$U_h\,(x;t) = P_x\; P_v\; f\;(\boldsymbol{x},\boldsymbol{v};t)\,, \tag{2.1}$$

and the second approach (the kinetic approach) can be expressed as

$$U_k\,(x;t) = P_v\; P_x\; f\;(\boldsymbol{x},\boldsymbol{v};t)\,. \tag{2.2}$$

In the above, P_x denotes a space-filtering projection operator, while P_v denotes the velocity projector associated with Chapman–Enskog expansion (Succi 2020). For turbulence modelling, these two projectors do not commute, which indicates the potential of the kinetic approach to yield new turbulence models.

2.2. *The coarse-grained Fokker–Planck equation for turbulence*

2.2.1. *The microscopic Fokker–Planck equation*

At the microscopic level, the positions $\boldsymbol{x}^*(t)$ and velocities $\boldsymbol{c}^*(t)$ of molecules can be described using the Boltzmann equation. Alternatively, they can also be considered as a

https://doi.org/10.1017/jfm.2025.323 Published online by Cambridge University Press

stochastic diffusion process (Heinz 2003). This process can be represented by deriving an equation for the motion of a single molecule colliding with all other molecules, resulting in the Langevin equation (Langevin 1908). Assuming the neglect of possible contributions from external forces, the Langevin equation can be expressed as

$$\frac{\mathrm{d}x_i^*}{\mathrm{d}t} = c_i^*, \quad \frac{\mathrm{d}c_i^*}{\mathrm{d}t} = -\frac{1}{\tau_m}\left(c_i^* - u_i\right) + \sqrt{\frac{4e}{3\tau_m}}\frac{\mathrm{d}W_i}{\mathrm{d}t}. \tag{2.3}$$

Notably, the mean velocity u_i is equivalent to the fluid velocity measured on the hydrodynamic scale, in accordance with the ergodic theorem. According to (2.3), the molecular velocity is driven by a drift towards the hydrodynamic velocity and a stochastic noise term governed by the derivative of a Wiener process $W(t)$. A Wiener process is a Gaussian process with $\mathrm{d}W_i(t) = W_i(t+\mathrm{d}t) - W_i(t)$, $\langle \mathrm{d}W_i(t)\rangle \equiv 0$ and $\left\langle \mathrm{d}W_i(t)\,\mathrm{d}W_j(t)\right\rangle \equiv \mathrm{d}t\,\delta_{ij}$, where the angle brackets denote the expectation of the stochastic processes inside. Here, τ_m is a molecular relaxation time characterising the molecular velocity relaxation and is related to the molecular viscosity, while e is the sensible energy relevant to the intensity of molecular fluctuations. All molecular statistics can be obtained by directly solving (2.3). For an Eulerian description, (2.3) can be reformulated as an equivalent Fokker–Planck equation for the molecular velocity distribution function $f(c_i, x_i, t)$, i.e.

$$\frac{\partial f}{\partial t} + c_i\frac{\partial f}{\partial x_i} = \frac{1}{\tau_m}\frac{\partial}{\partial c_k}[f(c_k - u_k)] + \frac{2e}{3\tau_m}\frac{\partial^2 f}{\partial c_k\,\partial c_k}. \tag{2.4}$$

By multiplying (2.4) by the conservation variables and integrating the resulting equations over the velocity space, one obtains the conservation equations at the hydrodynamic level (Heinz 2004; Jenny *et al.* 2010; Singh & Ansumali 2015).

2.2.2. *The Fokker–Planck equation for turbulence*

Equation (2.3) or (2.4) holds at the finest level of resolution, namely from the macroscopic length scale L all the way down to the molecular mean free path scale λ. However, such a microscale description is computationally prohibitive for most turbulent flows. Thus a kinetic model for turbulence at the hydrodynamic level is highly required – one that omits the intricate details of molecular motions.

Although differences between kinetic theory and statistical turbulence theory exist, as Taylor (1935) pointed out, one can still leverage the fundamental similarities underlying both statistical phenomena. In Brownian stochastic processes, molecular dynamics is modelled using two characteristic times: a long characteristic time for the non-equilibrium degree of freedom, embedded in a drift term, and a short characteristic time for other degrees of freedom that are in equilibrium, embedded in the Wiener process of the diffusion term. In turbulent flows, eddies of various sizes intermingle, and the statistical properties of one fluid particle result from the combined influence of these different-sized eddies. This reveals certain similarities between turbulence and Brownian motion. In addition, it has been established that two statistically independent characteristic times exist in turbulence – a long one for lower wavenumbers, and a short one for higher wavenumbers. According to Kolmogorov's hypotheses (Kolmogorov 1962), these two characteristic times are sufficiently separated when the Reynolds number is large, enabling the application of Brownian statistics to describe turbulent flow.

Recently, the experiments by Chong *et al.* (2020) further demonstrate that vortices can be treated as Brownian particles in a rotating turbulent convective flow. Based on these observations, we propose the following Langevin equation for turbulent flow at the

https://doi.org/10.1017/jfm.2025.323 Published online by Cambridge University Press

hydrodynamic level:

$$\frac{\mathrm{d}x_i^*}{\mathrm{d}t} = u_i^*, \quad \frac{\mathrm{d}u_i^*}{\mathrm{d}t} = \frac{1}{\rho}\frac{\partial \sigma_{ij}}{\partial x_j} - \frac{1}{\tau_T}(u_i^* - \bar{u}_i) + \sqrt{\frac{4k}{3\tau_T}}\frac{\mathrm{d}W_i}{\mathrm{d}t}. \tag{2.5}$$

And the corresponding Fokker–Planck equation can be obtained as

$$\frac{\partial f}{\partial t} + u_i\frac{\partial f}{\partial x_i} + \frac{1}{\rho}\frac{\partial \sigma_{ij}}{\partial x_j}\frac{\partial f}{\partial u_i} = \frac{1}{\tau_T}\frac{\partial}{\partial u_k}[f(u_k - \bar{u}_k)] + \frac{2k}{3\tau_T}\frac{\partial^2 f}{\partial u_k\,\partial u_k}. \tag{2.6}$$

The analogy between molecular and turbulent motions provides the basis for this model. Unlike (2.3) and (2.4), the velocities in (2.5) and (2.6) are at the hydrodynamic scale. Here, $\bar{u}_i$ is the mean velocity at the average flow field scale according to the ergodic theorem. The distribution function $f(u_i, x_i, t)$ describes the occupancy probability of the fluid particles in the phase space. Fluctuations are characterised by energy and a characteristic relaxation time. It should be noted that for modelling turbulent motions, the molecular energy e and relaxation time scale τ_m in (2.3) and (2.4) are replaced by the turbulent kinetic energy k and the relaxation time τ_T for turbulence in (2.5) and (2.6). Notably, a term relevant to molecular viscous stress, defined as $\sigma_{ij} = -\overline{\rho c_i' c_j'}$, is introduced in (2.5) and (2.6) to ensure the correct transport of mean velocities. As demonstrated in Appendix A, by taking moments of (2.6), one obtains the RANS equations and a partially modelled Reynolds stress equation at the average flow field level.

By focusing on the probabilistic evolution of velocity fluctuations, the Fokker–Planck model, as shown in (2.6), effectively captures the statistical nature of turbulence. The drift and diffusion terms account for the integrated effects of eddy interactions. Specifically, the drift term reflects the mean flow behaviour or large-scale structures, corresponding to coherent eddies, and is modelled as a relaxation towards the mean velocity, with τ_T characterising the relaxation time scale. As will be demonstrated in §§ 2.3 and 2.4, τ_T can be related to the eddy viscosity with an appropriate choice. The diffusion term captures the random, small-scale velocity fluctuations that arise from the chaotic breakdown of larger structures. While coherent structures are dependent on flow conditions, Kolmogorov's hypotheses suggest that small-scale chaotic motions exhibit a surprising degree of independence from the larger scales. Thus these small-scale fluctuations are modelled using a Wiener process, with turbulent energy k controlling their intensity.

2.2.3. *Connection with the PDF method*

Pope (1985, 2001) derives the exact transport equation for $f(u_i, x_i, t)$ as a hydrodynamic description from the NS equations. He then proposes a generalised Langevin model (GLM) to close this transport equation, which is the well-known PDF method. The form of GLM can be expressed as

$$\frac{\mathrm{d}x_i^*}{\mathrm{d}t} = u_i^*, \quad \frac{\mathrm{d}u_i^*}{\mathrm{d}t} = \frac{1}{\rho}\frac{\partial \sigma_{ij}}{\partial x_j} + G_{ij}(u_j^* - \bar{u}_j) + \sqrt{C_0\varepsilon}\frac{\mathrm{d}W_i}{\mathrm{d}t}. \tag{2.7}$$

And the corresponding PDF transport equation is

$$\frac{\partial f}{\partial t} + u_i\frac{\partial f}{\partial x_i} + \frac{1}{\rho}\frac{\partial \sigma_{ij}}{\partial x_j}\frac{\partial f}{\partial u_i} = -\frac{\partial}{\partial u_i}\left[f G_{ij}\left(u_j - \bar{u}_j\right)\right] + \frac{1}{2}C_0\varepsilon\frac{\partial^2 f}{\partial u_k\,\partial u_k}. \tag{2.8}$$

In fact, the GLM is a family of models, where $G_{ij}(\boldsymbol{x}, t)$ and $C_0(\boldsymbol{x}, t)$ are coefficients that define each specific model. By calibrating these coefficients against a broad range of

https://doi.org/10.1017/jfm.2025.323 Published online by Cambridge University Press

experiments, Haworth & Pope (1986, 1987) develop a model that exhibits satisfactory performance in both homogeneous shear flow and free shear flows. Furthermore, it can be contracted to the isotropisation of production model (IPM). According to Fu & Pope (1994) and Pope (2001), the GLM can be considered a nonlinear extension of Reynolds stress transport models, such as Rotta's model (Rotta 1951) and the Launder–Reece–Rodi model (Launder *et al.* 1975). Fu & Pope (1994) derive the Reynolds stress transport model corresponding to the Haworth–Pope model, and assess its performance in complex flow conditions induced by strong swirl. The results are compared with those from IPM and the k-ε model, revealing that the IPM demonstrates the best agreement with experimental data regarding the size of the recirculation, while the Haworth–Pope model tends to produce an excessively strong recirculation. However, when it comes to the profiles of mean flow and turbulence quantities, none of the models outperforms the others significantly.

Notably, our proposed model exhibits a form similar to the GLM. If we specify G_{ij} as isotropic and the coefficient C_0 as

$$\begin{aligned} G_{ij} &= -\delta_{ij}/\tau_T, \\ C_0 &= \frac{4}{3\tau_T}\frac{k}{\varepsilon}, \end{aligned} \tag{2.9}$$

the GLM ((2.7) and (2.8)) recovers (2.5) and (2.6). This implies that our proposed Fokker–Planck equation for turbulence can also be regarded as a specific instance of the GLM. In the next two subsections, the connection between the turbulent Fokker–Planck equation and the Reynolds stress constitutive relationship will be established.

2.3. *First-order expansion: linear EVMs*

Building on the derivation by Chen *et al.* (2004) for the BGK model, we employ a Chapman–Enskog expansion technique (Chapman & Cowling 1990) to derive turbulence models from the Fokker–Planck equation for turbulence, as illustrated in (2.6). We first use a reference velocity u_r, a reference collision time τ_r and a reference length L to non-dimensionalise (2.6) as

$$\frac{\partial \hat{f}}{\partial \hat{t}} + \hat{u}_j \frac{\partial \hat{f}}{\partial \hat{x}_j} + \frac{1}{\hat{\rho}} \frac{\partial \hat{\sigma}_{ij}}{\partial \hat{x}_i} \frac{\partial \hat{f}}{\partial \hat{u}_j} = \frac{1}{\hat{\tau}_T} \frac{\partial}{\partial \hat{u}_i} \left(\hat{u}_i' \hat{f} + \frac{2}{3} \hat{k} \frac{\partial \hat{f}}{\partial \hat{u}_i} \right) \frac{1}{\xi}. \tag{2.10}$$

In (2.10), u' is the fluctuation velocity, and ξ is defined as

$$\xi = \frac{u_r \tau_r}{L}. \tag{2.11}$$

In essence, ξ represents the ratio of the unresolved scale of motion to the resolved one, and can therefore be interpreted as a Knudsen number based on turbulent fluctuations (Righi 2016). Notably, it vanishes when returning to the dimensional form. For simplicity, we will omit the caret placed over the symbol in the following context. If we assume that ξ is a small quantity less than unity, then we can expand f as the power series

$$f = f^{(0)} + \xi f^{(1)} + \xi^2 f^{(2)} + \cdots. \tag{2.12}$$

https://doi.org/10.1017/jfm.2025.323 Published online by Cambridge University Press

Substituting (2.12) into (2.10), we obtain

$$
\begin{aligned}
&-\frac{1}{\tau_T}\frac{\partial}{\partial u_i}\left[u_i' f^{(0)}+\frac{2}{3}k\frac{\partial f^{(0)}}{\partial u_i}\right]\\
&+\xi\left[\frac{\partial f^{(0)}}{\partial t}+u_i\frac{\partial f^{(0)}}{\partial x_i}+\frac{1}{\rho}\frac{\partial \sigma_{ij}}{\partial x_j}\frac{\partial f^{(0)}}{\partial u_i}-\frac{1}{\tau_T}\frac{\partial}{\partial u_i}\left(u_i' f^{(1)}+\frac{2}{3}k\frac{\partial f^{(1)}}{\partial u_i}\right)\right]\\
&+\xi^2\left[\frac{\partial f^{(1)}}{\partial t}+u_i\frac{\partial f^{(1)}}{\partial x_i}+\frac{1}{\rho}\frac{\partial \sigma_{ij}}{\partial x_j}\frac{\partial f^{(1)}}{\partial u_i}-\frac{1}{\tau_T}\frac{\partial}{\partial u_i}\left(u_i' f^{(2)}+\frac{2}{3}k\frac{\partial f^{(2)}}{\partial u_i}\right)\right]=o(\xi^3).
\end{aligned}
\tag{2.13}
$$

Note that $f^{(0)}$ is an equilibrium distribution that does not include the non-trivial flow-induced fluctuations. Following the previous work of Chen *et al.* (2003, 2004), it is reasonable to use a local Gaussian form, specifically the Maxwell distribution

$$
f^{(0)}=\frac{n}{(4/3\pi k)^{3/2}}\exp\left(-\frac{\boldsymbol{u}'^2}{4k/3}\right),
\tag{2.14}
$$

to represent $f^{(0)}$. Notably, measurements from experiments and DNS in homogeneous turbulence (Tavoularis & Corrsin 1981; Yeung & Pope 1989) indicate that the one-point velocity distribution function is indeed jointly normal. Consequently, we find that the first term of (2.13) vanishes.

We further expand the time derivation as

$$
\begin{cases}
\dfrac{\partial f^{(0)}}{\partial t}=\dfrac{\partial_0 f^{(0)}}{\partial t}+\xi\dfrac{\partial_1 f^{(0)}}{\partial t}+\xi^2\dfrac{\partial_2 f^{(0)}}{\partial t}+\cdots,\\
\dfrac{\partial f^{(1)}}{\partial t}=\dfrac{\partial_0 f^{(1)}}{\partial t}+\xi\dfrac{\partial_1 f^{(1)}}{\partial t}+\xi^2\dfrac{\partial_2 f^{(1)}}{\partial t}+\cdots.
\end{cases}
\tag{2.15}
$$

Substituting (2.15) into (2.13), after rearrangement we obtain

$$
\begin{aligned}
&\left[\frac{\partial_0 f^{(0)}}{\partial t}+u_i\frac{\partial f^{(0)}}{\partial x_i}+\frac{1}{\rho}\frac{\partial \sigma_{ij}}{\partial x_j}\frac{\partial f^{(0)}}{\partial u_i}-\frac{1}{\tau_T}\frac{\partial}{\partial u_i}\left(u_i' f^{(1)}+\frac{2}{3}k\frac{\partial f^{(1)}}{\partial u_i}\right)\right]\\
&+\xi\left[\frac{\partial_1 f^{(0)}}{\partial t}+\frac{\partial_0 f^{(1)}}{\partial t}+u_i\frac{\partial f^{(1)}}{\partial x_i}+\frac{1}{\rho}\frac{\partial \sigma_{ij}}{\partial x_j}\frac{\partial f^{(1)}}{\partial u_i}-\frac{1}{\tau_T}\frac{\partial}{\partial u_i}\left(u_i' f^{(2)}+\frac{2}{3}k\frac{\partial f^{(2)}}{\partial u_i}\right)\right]\\
&=o(\xi^2).
\end{aligned}
\tag{2.16}
$$

Consequently, (2.10) is transformed into an infinite hierarchy of equations based of the order of ξ. In particular,

$$
f^{(0)}=f_M=\frac{n}{(4/3\pi k)^{3/2}}\exp\left(-\frac{\boldsymbol{u}'^2}{4k/3}\right),
\tag{2.17}
$$

$$
\frac{\partial}{\partial u_i}\left(u_i' f^{(1)}+\frac{2}{3}k\frac{\partial f^{(1)}}{\partial u_i}\right)=\tau_T\left(\frac{\partial_0 f^{(0)}}{\partial t}+u_i\frac{\partial f^{(0)}}{\partial x_i}+\frac{1}{\rho}\frac{\partial \sigma_{ij}}{\partial x_j}\frac{\partial f^{(0)}}{\partial u_i}\right),
\tag{2.18}
$$

https://doi.org/10.1017/jfm.2025.323 Published online by Cambridge University Press

$$\frac{\partial}{\partial u_i}\left(u_i' f^{(2)} + \frac{2}{3}k\frac{\partial f^{(2)}}{\partial u_i}\right) = \tau_T\left(\frac{\partial_1 f^{(0)}}{\partial t} + \frac{\partial_0 f^{(1)}}{\partial t} + u_i\frac{\partial f^{(1)}}{\partial x_i} + \frac{1}{\rho}\frac{\partial \sigma_{ij}}{\partial x_j}\frac{\partial f^{(1)}}{\partial u_i}\right). \tag{2.19}$$

Next, we will determine the solution corresponding to the first-order expansion. Since the spatial and time dependence of $f^{(0)}$ is only through ρ, $\bar{u}_i$ and k, we can organise the right-hand side of (2.18) into

$$\begin{aligned}
&\tau_T\left(\frac{\partial_0 f^{(0)}}{\partial t} + u_i\frac{\partial f^{(0)}}{\partial x_i} + \frac{1}{\rho}\frac{\partial \sigma_{ij}}{\partial x_j}\frac{\partial f^{(0)}}{\partial u_i}\right)\\
&\quad = \tau_T\left[\frac{\partial f^{(0)}}{\partial \rho}\left(\frac{\partial_0 \rho}{\partial t} + u_j\frac{\partial \rho}{\partial x_j}\right) + \frac{\partial f^{(0)}}{\partial \bar{u}_i}\left(\frac{\partial_0 \bar{u}_i}{\partial t} + u_j\frac{\partial \bar{u}_i}{\partial x_j}\right)\right.\\
&\qquad \left. + \frac{\partial f^{(0)}}{\partial k}\left(\frac{\partial_0 k}{\partial t} + u_j\frac{\partial k}{\partial x_j}\right) - \frac{1}{\rho}\frac{\partial \sigma_{ij}}{\partial x_j} \times f^{(0)}\frac{u_i'}{2k/3}\right].
\end{aligned} \tag{2.20}$$

Using the expression for $f^{(0)}$, it can be demonstrated directly that

$$\begin{cases}
\dfrac{\partial f^{(0)}}{\partial \rho} = \dfrac{f^{(0)}}{\rho},\\[2ex]
\dfrac{\partial f^{(0)}}{\partial \bar{u}_i} = f^{(0)}\dfrac{u_i'}{2k/3},\\[2ex]
\dfrac{\partial f^{(0)}}{\partial k} = f^{(0)}\left[\dfrac{u_i'u_i'}{4k^2/3} - \dfrac{3}{2k}\right].
\end{cases} \tag{2.21}$$

For the time derivation terms involved in (2.20), we will use the RANS equation and the governing equation of k, i.e.

$$\begin{cases}
\dfrac{\partial \rho}{\partial t} = -\rho\dfrac{\partial \bar{u}_j}{\partial x_j} - \bar{u}_j\dfrac{\partial \rho}{\partial x_j},\\[2ex]
\dfrac{\partial \bar{u}_i}{\partial t} = -\bar{u}_j\dfrac{\partial \bar{u}_i}{\partial x_j} + \dfrac{1}{\rho}\dfrac{\partial \sigma_{ij}}{\partial x_j} + \dfrac{1}{\rho}\dfrac{\partial \sigma_{ij}^T}{\partial x_j},\\[2ex]
\dfrac{\partial k}{\partial t} = -\bar{u}_j\dfrac{\partial k}{\partial x_j} + \dfrac{1}{\rho}\sigma_{ij}^T\dfrac{\partial \bar{u}_i}{\partial x_j} - \dfrac{\partial}{\partial x_j}\left(\nu_{eff}^k\dfrac{\partial k}{\partial x_j}\right) - \varepsilon.
\end{cases} \tag{2.22}$$

In the above equations, $\nu_{eff}^k = \nu + \nu_T/\sigma_k$ is the effective diffusivity for k, and $\sigma_{ij}^T = -\overline{\rho u_i' u_j'}$ is the Reynolds stress. We can expand σ_{ij}^T into a power series as

$$\sigma_{ij}^T = -\frac{2}{3}\rho k\delta_{ij} + \sigma_{ij}^{T(0)} + \xi\sigma_{ij}^{T(1)} + \xi^2\sigma_{ij}^{T(2)} + \cdots, \tag{2.23}$$

where $\sigma_{ij}^{T(\alpha)} = -\int_{R^3} m u_{\langle i}' u_{j\rangle}' f^{(\alpha)}\,\mathrm{d}\boldsymbol{u}$. Notably, to enhance clarity and conciseness, we use angle brackets to denote the symmetric and deviatoric (or trace-free) part of the tensor. Its complete form is given by

$$u_{\langle i}' u_{j\rangle}' = \frac{1}{2}(u_i'u_j' + u_j'u_i') - \frac{1}{3}u_k'u_k'\delta_{ij}. \tag{2.24}$$

https://doi.org/10.1017/jfm.2025.323 Published online by Cambridge University Press

Additionally, the Einstein summation convention is applied here and throughout the text. It is easy to demonstrate that

$$\sigma_{ij}^{T(0)} = -\int_{R^3} m u'_{\langle i} u'_{j\rangle} f^{(0)}\, \mathrm{d}\boldsymbol{u} = 0. \tag{2.25}$$

Thus

$$\sigma_{ij}^{T} = -\frac{2}{3}\rho k \delta_{ij} + \xi \sigma_{ij}^{T(1)} + \xi^2 \sigma_{ij}^{T(2)} + \cdots . \tag{2.26}$$

Substituting (2.26) into (2.22), we obtain

$$\begin{cases} \dfrac{\partial \rho}{\partial t} = -\rho \dfrac{\partial \bar{u}_j}{\partial x_j} - \bar{u}_j \dfrac{\partial \rho}{\partial x_j}, \\ \dfrac{\partial \bar{u}_i}{\partial t} = -\bar{u}_j \dfrac{\partial \bar{u}_i}{\partial x_j} + \dfrac{1}{\rho}\dfrac{\partial \sigma_{ij}}{\partial x_j} - \dfrac{1}{\rho}\dfrac{2}{3}\dfrac{\partial \rho k \delta_{ij}}{\partial x_j} + \dfrac{1}{\rho}\displaystyle\sum_{\alpha} \xi^{\alpha} \dfrac{\partial \sigma_{ij}^{T(\alpha)}}{\partial x_j}, \\ \dfrac{\partial k}{\partial t} = -\bar{u}_j \dfrac{\partial k}{\partial x_j} - \dfrac{1}{\rho}\cdot\dfrac{2}{3}\rho k \dfrac{\partial \bar{u}_i}{\partial x_j}\delta_{ij} + \dfrac{1}{\rho}\displaystyle\sum_{\alpha} \xi^{\alpha} \sigma_{ij}^{T(\alpha)} \dfrac{\partial \bar{u}_i}{\partial x_j} - \nu_{eff}^{k} \dfrac{\partial^2 k}{\partial {x_j}^2} - \varepsilon. \end{cases} \tag{2.27}$$

In this manner, the time derivation of ρ, $\bar{u}_i$ and k can be expanded in a power series as

$$\begin{cases} \dfrac{\partial_0 \rho}{\partial t} = -\rho \dfrac{\partial \bar{u}_j}{\partial x_j} - \bar{u}_j \dfrac{\partial \rho}{\partial x_j}, \\ \dfrac{\partial_0 \bar{u}_i}{\partial t} = -\bar{u}_j \dfrac{\partial \bar{u}_i}{\partial x_j} + \dfrac{1}{\rho}\dfrac{\partial \sigma_{ij}}{\partial x_j} - \dfrac{1}{\rho}\dfrac{2}{3}\dfrac{\partial \rho k}{\partial x_i}, \qquad (\alpha = 0)\,, \\ \dfrac{\partial_0 k}{\partial t} = -\bar{u}_j \dfrac{\partial k}{\partial x_j} - \dfrac{1}{\rho}\dfrac{2}{3}\rho k \dfrac{\partial \bar{u}_i}{\partial x_i} - \nu_{eff}^{k} \dfrac{\partial^2 k}{\partial {x_j}^2} - \varepsilon, \end{cases} \tag{2.28}$$

$$\begin{cases} \dfrac{\partial_\alpha \rho}{\partial t} = 0, \\ \dfrac{\partial_\alpha \bar{u}_i}{\partial t} = \dfrac{1}{\rho}\xi^{\alpha} \dfrac{\partial \sigma_{ij}^{T(\alpha)}}{\partial x_j}, \qquad (\alpha \geqslant 1)\,. \\ \dfrac{\partial_\alpha k}{\partial t} = \dfrac{1}{\rho}\xi^{\alpha} \sigma_{ij}^{T(\alpha)} \dfrac{\partial \bar{u}_i}{\partial x_j}. \end{cases} \tag{2.29}$$

Substituting (2.21) and (2.28) into (2.20), and omitting terms that are associated with the second derivative of k and ε for simplicity, we then obtain

$$\begin{aligned} &\tau_T \left(\frac{\partial_0 f^{(0)}}{\partial t} + u_i \frac{\partial f^{(0)}}{\partial x_i} + \frac{1}{\rho}\frac{\partial \sigma_{ij}}{\partial x_j}\frac{\partial f^{(0)}}{\partial u_i} \right) \\ &\quad = \frac{\tau_T}{2k/3} f^{(0)} \left[\left(u'_i u'_j \frac{\partial \bar{u}_i}{\partial x_j} - \frac{1}{3} u'_i u'_i \frac{\partial \bar{u}_j}{\partial x_j} \right) + u'_j \left(\frac{\boldsymbol{u}'^2}{2} - \frac{5}{2}\cdot\frac{2}{3}k \right) \frac{\partial \ln k}{\partial x_j} \right]. \end{aligned} \tag{2.30}$$

https://doi.org/10.1017/jfm.2025.323 Published online by Cambridge University Press

We can transform the left-hand side of (2.18) into

$$\frac{\partial}{\partial u_i}\left(u_i' f^{(1)} + \frac{2}{3}k\frac{\partial f^{(1)}}{\partial u_i}\right) = \frac{\partial}{\partial u_i}\left[\frac{2}{3}k\, f_M \frac{\partial}{\partial u_i}\left(\frac{f^{(1)}}{f_M}\right)\right]. \tag{2.31}$$

Combining with (2.30), (2.18) can be written as

$$\begin{aligned}&\frac{1}{f_M}\frac{\partial}{\partial u_i}\left[\frac{2}{3}k\, f_M \frac{\partial}{\partial u_i}\left(\frac{f^{(1)}}{f_M}\right)\right]\\ &\quad = \frac{\tau_T}{2k/3}\left[\left(u_i' u_j' \frac{\partial \bar{u}_i}{\partial x_j} - \frac{1}{3}u_i' u_i' \frac{\partial \bar{u}_j}{\partial x_j}\right) + u_j'\left(\frac{\boldsymbol{u}'^2}{2} - \frac{5}{2}\frac{2}{3}k\right)\frac{\partial \ln k}{\partial x_j}\right].\end{aligned} \tag{2.32}$$

The left-hand side of (2.32) is a linear operator of $f^{(1)}/f_M$, so we can denote it as $L[f^{(1)}/f_M]$. If we define

$$A_{ij} = u_i' u_j' - \frac{1}{3}u_k' u_k' \delta_{ij}, \tag{2.33}$$

$$B_j = u_j'\left(\frac{\boldsymbol{u}'^2}{2} - \frac{5}{2}\frac{2}{3}k\right), \tag{2.34}$$

then (2.32) can be simplified as

$$L\left[\frac{f^{(1)}}{f_M}\right] = \frac{\tau_T}{2k/3}\left[A_{ij}\frac{\partial \bar{u}_i}{\partial x_j} + B_j \frac{\partial \ln k}{\partial x_j}\right]. \tag{2.35}$$

Notably, it is easy to demonstrate that A_{ij} and B_j are eigenfunctions of operator $L[\,]$, specifically,

$$\begin{aligned}L\left[A_{ij}\right] &= -2A_{ij},\\ L\left[B_j\right] &= -3B_j.\end{aligned} \tag{2.36}$$

So $f^{(1)}$ must be a linear combination of A_{ij} and B_j. We can assume the form of $f^{(1)}$ as

$$\frac{f^{(1)}}{f_M} = \frac{\tau_T}{2k/3}\left(a\, A_{ij} + b\, B_j\right), \tag{2.37}$$

and the parameters can be determined easily, i.e.

$$\begin{aligned}a &= -\frac{1}{2}\frac{\partial \bar{u}_i}{\partial x_j},\\ b &= -\frac{1}{3}\frac{\partial \ln k}{\partial x_j}.\end{aligned} \tag{2.38}$$

Consequently, we obtain the expression for $f^{(1)}$as

$$f^{(1)} = f_M \frac{\tau_T}{2k/3}\left[-\frac{1}{2}\left(u_i' u_j' - \frac{1}{3}u_k' u_k' \delta_{ij}\right)\frac{\partial \bar{u}_i}{\partial x_j} - \frac{1}{3}u_j'\left(\frac{\boldsymbol{u}'^2}{2} - \frac{5}{2}\frac{2}{3}k\right)\frac{\partial \ln k}{\partial x_j}\right]. \tag{2.39}$$

The first-order approximation of Reynolds stress can be determined by taking moments of $f^{(1)}$, i.e.

$$\sigma_{ij}^{T(1)} = -\int_{R^3} m u_{\langle i}' u_{j\rangle}' f^{(1)}\, \mathrm{d}\boldsymbol{u}' = \frac{\tau_T}{2}\rho\frac{2}{3}k\left[\frac{\partial \bar{u}_i}{\partial x_j} + \frac{\partial \bar{u}_j}{\partial x_i} - \frac{2}{3}\frac{\partial \bar{u}_k}{\partial x_k}\delta_{ij}\right]. \tag{2.40}$$

https://doi.org/10.1017/jfm.2025.323 Published online by Cambridge University Press

If τ_T is determined by $3\nu_T/k$, then (2.40) together with the isotropic part $-2/3\rho k$ is exactly the linear EVM, i.e.

$$\sigma_{ij}^T = -\frac{2}{3}\rho k\delta_{ij} + 2\rho\nu_T S_{ij}^d, \tag{2.41}$$

where S_{ij}^d is the strain tensor of the mean flow, i.e.

$$S_{ij}^d = \frac{1}{2}\frac{\partial \bar{u}_i}{\partial x_j} + \frac{1}{2}\frac{\partial \bar{u}_j}{\partial x_i} - \frac{1}{3}\frac{\partial \bar{u}_k}{\partial x_k}\delta_{ij}. \tag{2.42}$$

2.4. *Second-order expansion: nonlinear EVMs*

As noted in the previous subsection, the parameter ξ can be regarded as a Knudsen number for turbulence, with the Boussinesq approximation's applicability relying on it being small. The linear EVM offers a limited representation of anisotropy and is effective only for simple shear flows. To some extent, a mean turbulent flow more closely resembles a flow with a finite Knudsen number (Wilcox 1998). For example, when the Reynolds number exceeds 20,000, an overlap region exists between the inner layer ($y < 0.1\delta$) and the outer layer ($y > 50\delta_v$) of the boundary layer (Pope 2001), where y denotes the distance from the wall. Here, δ represents the boundary layer thickness, while δ_v is the viscosity scale, defined as $\delta_v \equiv \nu\sqrt{\rho/\tau_w}$, ν denotes the kinematic viscosity, ρ is the density, and τ_w is the wall shear stress. In this region, the characteristic length scale of large-scale turbulent eddies L, given by $L \equiv k^{3/2}/\varepsilon$, and the mixing length l_{mix} both vary linearly with y (Wilcox 1998; Pope 2001). The proportionality constant for L/y is approximately 2.5, while that for l_{mix}/y corresponds to the Kármán constant, $\kappa \approx 0.41$. Consequently, the turbulent Knudsen number is typically of order 1, i.e.

$$Kn = \frac{l_{mix}}{L} = \frac{0.41\,y}{2.5y} \approx 0.164. \tag{2.43}$$

This implies that the contributions from higher-order terms become non-negligible. To enhance the representation of Reynolds stress anisotropy, we next expand the turbulent Fokker–Planck equation to second order.

Starting with (2.19) and applying calculations similar to those in the previous subsection, we can reorganise (2.19) as

$$\frac{1}{f_M}\frac{\partial}{\partial u_i}\left[\frac{2}{3}k\, f_M \frac{\partial}{\partial u_i}\left(\frac{f^{(2)}}{f_M}\right)\right] = -\frac{1}{2}\frac{\tau_T^2}{2k/3}\left[-(E_1+E_2) + A + B + C + D\right], \tag{2.44}$$

where

$$\begin{aligned} E_1 &= 2\times\frac{2}{3}k\times u_i'\frac{\partial S_{ij}^d}{\partial x_j}, \\ E_2 &= 2\times\frac{2}{3}k\times\frac{1}{3}\left(\frac{u_i'u_i'}{4k/3} - \frac{3}{2}\right)\times 2S_{ij}^d\frac{\partial \bar{u}_i}{\partial x_j}, \\ A &= \frac{1}{2k/3}\left[\left(u_i'u_j' - \frac{1}{3}u_k'u_k'\delta_{ij}\right)\frac{\partial \bar{u}_i}{\partial x_j}\right]^2, \end{aligned}$$

https://doi.org/10.1017/jfm.2025.323 Published online by Cambridge University Press

$$
\begin{aligned}
B &= \left[\frac{\partial_0}{\partial t}\left(\frac{\partial \bar{u}_i}{\partial x_j}\right)+\bar{u}_l\frac{\partial}{\partial x_l}\left(\frac{\partial \bar{u}_i}{\partial x_j}\right)\right]\times\left(u_i'u_j'-\frac{1}{3}u_k'u_k'\delta_{ij}\right)\\
&\quad+u_l'\frac{\partial}{\partial x_l}\left(\frac{\partial \bar{u}_i}{\partial x_j}\right)\times\left(u_i'u_j'-\frac{1}{3}u_k'u_k'\delta_{ij}\right),\\
C &= -\left[u_l'u_j'\frac{\partial \bar{u}_i}{\partial x_l}+u_l'u_i'\frac{\partial \bar{u}_j}{\partial x_l}-\frac{2}{3}u_k'u_l'\frac{\partial \bar{u}_k}{\partial x_l}\delta_{ij}\right]\frac{\partial \bar{u}_i}{\partial x_j},\\
D &= -\frac{1}{\rho}\frac{\partial \sigma_{lj}}{\partial x_j}\left[\frac{u_l'}{2k/3}\times\left(u_i'u_j'-\frac{1}{3}u_k'u_k'\delta_{ij}\right)\frac{\partial \bar{u}_i}{\partial x_j}\right.\\
&\quad\left.+\left(u_j'\frac{\partial \bar{u}_l}{\partial x_j}+u_i'\frac{\partial \bar{u}_i}{\partial x_l}-\frac{2}{3}u_l'\delta_{ij}\frac{\partial \bar{u}_i}{\partial x_j}\right)\right].
\end{aligned}
\tag{2.45}
$$

We further express (2.44) in terms of the eigenfunctions, with the expressions of the eigenfunctions provided in Appendix B, as

$$
\begin{aligned}
L\left[\frac{f^{(2)}}{f_M}\right]=&-\frac{1}{2}\frac{\tau_T^2}{2k/3}\left\{-\frac{4}{3}k\,Q_{E_1}-\frac{8}{9}k\,S_{ij}^d\frac{\partial \bar{u}_i}{\partial x_j}\,Q_{E_2}+\frac{1}{2k/3}\,Q_A\right.\\
&\left.+\left[\frac{\partial_0}{\partial t}\left(\frac{\partial \bar{u}_i}{\partial x_j}\right)+\bar{u}_l\frac{\partial}{\partial x_l}\left(\frac{\partial \bar{u}_i}{\partial x_j}\right)\right]Q_{B_1}+Q_{B_2}-Q_C-\frac{1}{2k/3}Q_{D_1}-Q_{D_2}\right\}.
\end{aligned}
\tag{2.46}
$$

We can assume that $f^{(2)}$ is the combination of eigenfunctions of the Fokker–Planck operator, i.e.

$$
\begin{aligned}
\frac{f^{(2)}}{f_M}=&-\frac{1}{2}\frac{\tau_T^2}{2k/3}\left(pQ_{E_1}+qQ_{E_2}+xQ_A+yQ_{B_1}+zQ_{B_2}\right.\\
&\left.+uQ_C+vQ_{D_1}+wQ_{D_2}+mD+nM\right),
\end{aligned}
\tag{2.47}
$$

where $p, q, x, y, z, u, v, w, m, n$ are parameters that need to be determined. By substituting (2.47) into the Fokker–Planck operator and using the relationships provided in Appendix B, we find that

$$
\begin{aligned}
L\left[\frac{f^{(2)}}{f_M}\right]=&-\frac{1}{2}\frac{\tau_T^2}{2k/3}\left[-p\cdot Q_{E_1}-2q\cdot Q_{E_2}-4x\cdot Q_A-2y\cdot Q_{B_1}-3z\cdot Q_{B_2}-2u\cdot Q_C\right.\\
&-3v\cdot Q_{D_1}+\left(\frac{4}{3}k\cdot v-w\right)Q_{D_2}+\left(\frac{4}{3}k\cdot z-m\right)\cdot D\\
&\left.+\left(\frac{4}{3}k\cdot x-2n\right)\cdot M+\left(\frac{4}{3}k\cdot u+\frac{8}{3}k\cdot n\right)\cdot N\right].
\end{aligned}
\tag{2.48}
$$

By comparing (2.48) with (2.46), we obtain eleven equations for the ten unknown parameters. Evidently, these equations are consistent, and the parameters can be

https://doi.org/10.1017/jfm.2025.323 Published online by Cambridge University Press

determined as

$$p=\frac{4}{3}k,\quad q=\frac{4}{9}k\cdot S_{ij}^{d}\frac{\partial\bar{u}_i}{\partial x_j},\quad x=-\frac{1}{8k/3},\quad y=-\frac{1}{2}\left[\frac{\partial_0}{\partial t}\left(\frac{\partial\bar{u}_i}{\partial x_j}\right)+\bar{u}_l\frac{\partial}{\partial x_l}\left(\frac{\partial\bar{u}_i}{\partial x_j}\right)\right],$$
$$z=-\frac{1}{3},\quad u=\frac{1}{2},\quad v=\frac{1}{2k},\quad w=\frac{5}{3},\quad m=-\frac{4}{9}k,\quad n=-\frac{1}{4}. \tag{2.49}$$

So far, we have derived the expression for $f^{(2)}$, i.e.

$$f^{(2)}=\frac{1}{2}\frac{\tau_T^2}{2k/3}\cdot f_M\left(-\frac{4}{3}k\cdot Q_{E_1}-\frac{4}{9}k\cdot S_{ij}^{d}\frac{\partial\bar{u}_i}{\partial x_j}\cdot Q_{E_2}+\frac{1}{8k/3}\cdot Q_A\right.$$
$$+\frac{1}{2}\left[\frac{\partial_0}{\partial t}\left(\frac{\partial\bar{u}_i}{\partial x_j}\right)+\bar{u}_l\frac{\partial}{\partial x_l}\left(\frac{\partial\bar{u}_i}{\partial x_j}\right)\right]\cdot Q_{B_1}+\frac{1}{3}\cdot Q_{B_2}$$
$$\left.-\frac{1}{2}\cdot Q_C-\frac{1}{2k}Q_{D_1}-\frac{5}{3}Q_{D_2}+\frac{4}{9}k\cdot D+\frac{1}{4}\cdot M\right). \tag{2.50}$$

The second-order expansion of Reynolds stress can be obtained by taking moments of $f^{(2)}$ term by term, with the relevant integrals presented in Appendix C. After reorganisation, the result can be expressed as

$$\sigma_{ij}^{T(2)}=-\frac{1}{2}\rho\tau_T^2\cdot\left(\frac{2}{3}k\right)\cdot\left(\frac{\partial_0}{\partial t}+\bar{u}_k\frac{\partial}{\partial x_k}\right)S_{ij}^{d}$$
$$-\rho\tau_T^2\cdot\left(\frac{2}{3}k\right)\cdot\left(S_{ik}^{d}S_{kj}^{d}-\frac{1}{3}S_{mn}^{d}S_{mn}^{d}\delta_{ij}\right)+\frac{1}{2}\rho\tau_T^2\cdot\left(\frac{2}{3}k\right)\cdot(S_{ik}^{d}\Omega_{kj}+S_{jk}^{d}\Omega_{ki}). \tag{2.51}$$

The turbulent relaxation time τ_T can be related to the eddy viscosity ν_T according to the relationship

$$\nu_T=\frac{\tau_T}{2}\cdot\frac{2}{3}k, \tag{2.52}$$

which is consistent with the first-order expansion. In this way, (2.51) can be expressed in a more formal manner, i.e.

$$\sigma_{ij}^{T(2)}=-2\rho\frac{\nu_T^2}{2k/3}\cdot\left(\frac{\partial_0}{\partial t}+\bar{u}_k\frac{\partial}{\partial x_k}\right)S_{ij}^{d}$$
$$-4\rho\frac{\nu_T^2}{2k/3}\cdot\left(S_{ik}^{d}S_{kj}^{d}-\frac{1}{3}S_{mn}^{d}S_{mn}^{d}\delta_{ij}\right)+2\rho\frac{\nu_T^2}{2k/3}\cdot(S_{ik}^{d}\Omega_{kj}+S_{jk}^{d}\Omega_{ki}). \tag{2.53}$$

In (2.53), Ω_{ij} is the vorticity tensor of the mean velocity field, which is defined as

$$\Omega_{ij}\equiv\frac{1}{2}\left(\frac{\partial\bar{u}_i}{\partial x_j}-\frac{\partial\bar{u}_j}{\partial x_i}\right). \tag{2.54}$$

This second-order expansion, as shown in (2.53), provides a more accurate representation of the Reynolds stress by including the effects of higher-order velocity gradients, which are essential for capturing complex turbulent behaviours such as secondary flow in a square duct.

https://doi.org/10.1017/jfm.2025.323 Published online by Cambridge University Press

3. Results and validation

Ignoring terms associated with ν_{eff}^{k}, ε and the derivations of k, the Reynolds stress based on the turbulent Fokker–Planck equation is given by

truncated to zeroth order,

$$\sigma_{ij}^{T} \approx -\frac{2}{3}\rho k\delta_{ij},$$

truncated to first order,

$$\sigma_{ij}^{T} \approx -\frac{2}{3}\rho k\delta_{ij} + 2\rho\nu_T S_{ij}^{d},$$

truncated to second order,

$$\sigma_{ij}^{T} \approx -\frac{2}{3}\rho k\delta_{ij} + 2\rho\nu_T S_{ij}^{d} - 2\rho\frac{\nu_T^2}{2k/3}\cdot\left(\frac{\partial_0}{\partial t} + \bar{u}_k\frac{\partial}{\partial x_k}\right)S_{ij}^{d} - 4\rho\frac{\nu_T^2}{2k/3}\cdot\left(S_{ik}^{d}S_{kj}^{d} - \frac{1}{3}S_{mn}^{d}S_{mn}^{d}\delta_{ij}\right) + 2\rho\frac{\nu_T^2}{2k/3}\cdot(S_{ik}^{d}\Omega_{kj} + S_{jk}^{d}\Omega_{ki}). \tag{3.1}$$

When truncated to zeroth order, the obtained solution corresponds to the isotropic part of the Reynolds stress. Truncating to first order recovers the linear EVM, which offers an insufficient representation of anisotropy and is primarily effective for simple shear flows. When extending the truncation to second order, the resulting quadratic Reynolds stress constitutive relationship closely mirrors the form of NLEVMs, providing a more accurate description of turbulent anisotropy. Additionally, a history effect is revealed by the material derivative of the strain tensor, which may be effective for flows with sudden changes in the mean strain rate. Notably, this constitutive relationship is applicable to regions outside the viscous sublayer. By applying direction-specific damping functions, the near-wall asymptotic behaviour of normal Reynolds stress anisotropy can be effectively preserved. This approach has been demonstrated successfully by Apsley & Leschziner (1998), Rung *et al.* (1998), Wallin & Johansson (2000) and Fu *et al.* (2003), showing significant effectiveness in low-Reynolds-number modifications. Interestingly, (3.1) closely aligns with the results obtained by Chen *et al.* (2004), differing mainly by the omission of the molecular viscous term in their coarse-grained BGK model.

To further validate the effectiveness of (3.1), we compare the coefficients of (3.1) with those of typical quadratic NLEVMs in the literature. Subsequently, we implement (3.1) in computational fluid dynamics (CFD) codes, and compare the results with experimental data to evaluate the model's ability to accurately reproduce physical phenomena.

3.1. *Comparison of the coefficients*

Truncated to quadratic terms, the basic stress–strain relationship can be written in a normalised anisotropic form as

https://doi.org/10.1017/jfm.2025.323 Published online by Cambridge University Press

Model	C_μ	C_1	C_2	C_3	Additional terms
Speziale (1987)	0.09	-6.72	0	0	$-0.6\frac{\nu_T}{\varepsilon}(\dot{S}_{ij}-\frac{1}{3}\dot{S}_{kk}\delta_{ij})$
Nisizima & Yoshizawa (1987)	0.09	-33.78	8	46.22	–
Rubinstein & Barton (1990)	0.0845	32.19	6.63	-26.51	–
Myong & Kasagi (1990)	0.09	12.44	10.67	2.22	W_{ij}
Shih *et al.* (1993)	$(2/3)/(1.25+S+0.9\Omega)$	$(3/C_\mu^2)/(1000+S^3)$	$(15.2/C_\mu^2)/(1000+S^3)$	$(19.2/C_\mu^2)/(1000+S^3)$	–
Fu *et al.* (1997), Rung *et al.* (1998)	0.09*	10.22	4.66	0	–
Present model	0.09	6.0	3.0	0	D_{ij}

$S=(k/\varepsilon)\sqrt{2S_{ij}S_{ij}}$, $\Omega=(k/\varepsilon)\sqrt{2\Omega_{ij}\Omega_{ij}}$, $\dot{S}_{ij}=\frac{\partial S_{ij}}{\partial t}+\bar{u}_k\frac{\partial S_{ij}}{\partial x_k}-\frac{\partial \bar{u}_i}{\partial x_k}S_{kj}-\frac{\partial \bar{u}_j}{\partial x_k}S_{ki}$,

$W_{ij}=\frac{2}{3}\frac{\nu}{\varepsilon}\left(\frac{\partial\sqrt{k}}{\partial x_n}\right)^2\left(-\delta_{ij}-\delta_{in}\delta_{jn}+4\delta_{im}\delta_{jm}\right)$, $D_{ij}=-3\frac{\nu_T^2}{k^2}\left(\frac{\partial_0}{\partial t}+\bar{u}_k\frac{\partial}{\partial x_k}\right)S_{ij}^d$.

Table 1. Coefficients in typical quadratic NLEVMs.

*In the original model of Fu *et al.* (1997) and Rung *et al.* (1998), this coefficient depends on the local mean strain rates. For ease of comparison, it is set to 0.09 here.

$$\begin{aligned} a_{ij} &= \frac{\overline{\rho u_i u_j}-\frac{2}{3}\rho k\delta_{ij}}{\rho k} \\ &= -2\frac{\nu_T}{k}S_{ij}+C_1\frac{\nu_T^2}{k^2}\left(S_{ik}S_{kj}-\frac{1}{3}S_{kl}S_{kl}\delta_{ij}\right)+C_2\frac{\nu_T^2}{k^2}\left(\Omega_{ik}S_{kj}-S_{ik}\Omega_{kj}\right) \\ &\quad +C_3\frac{\nu_T^2}{k^2}\left(\Omega_{ik}\Omega_{jk}-\frac{1}{3}\Omega_{lk}\Omega_{lk}\delta_{ij}\right). \end{aligned} \tag{3.2}$$

For k-ε models, the turbulent viscosity ν_T can be determined by

$$\nu_T = C_\mu\frac{k^2}{\varepsilon}. \tag{3.3}$$

Note that there are four empirical coefficients in (3.2): C_μ, the usual coefficient employed in linear EVMs, and the coefficients of the quadratic terms, C_1, C_2 and C_3. Table 1 lists the proposed values for these coefficients in several typical quadratic NLEVMs.

Typically, the coefficients in NLEVMs are determined by considering the prediction of shear stress in simple shear flows or other complex flows. It is evident that the optimised sets of coefficients proposed for C_1-C_3 can vary significantly, depending on the specific flow or flow feature chosen for prediction. Remarkably, the present model, which is theoretically derived from the Fokker–Planck equation for turbulence, yields coefficients that are quantitatively close to those of established NLEVMs, particularly the quasi-realisable quadratic EVM of Fu *et al.* (1997) and Rung *et al.* (1998). Additionally, a notable feature of the present quadratic model is that there is no contribution from $\Omega_{ik}\Omega_{jk}-1/3\Omega_{lk}\Omega_{lk}\delta_{ij}$. This finding aligns with the prediction of Speziale (1987), which demonstrated that such a quadratic rate-of-rotation tensor contribution leads to erroneous predictions for isotropic turbulence subjected to a solid-body rotation.

https://doi.org/10.1017/jfm.2025.323 Published online by Cambridge University Press

3.2. *Comparison with experiments*

The performance of the present nonlinear model is evaluated across three test cases: one incompressible and two compressible. The calculations are performed using the open-source software OpenFOAM (Jasak *et al.* 2007), version 10. For the incompressible case, the solver simpleFoam is utilised. For the compressible cases, we use a modified density-based solver, ausmpwTurbulentFoam (Zhang 2021), which is adapted from rhoCentralFoam (Greenshields *et al.* 2010) and employs the AUSMPW+ scheme (Kim *et al.* 2001) for the convection terms to reduce numerical dissipation. The remaining terms are discretised similarly to those in rhoCentralFoam. Specifically, a second-order central scheme is applied for diffusion terms, while a second-order total variation diminishing method with the van Albada *et al.* (1982) limiter is used for cell face interpolations to ensure solution boundedness.

The new models are implemented based on two well-established k-ε models: the Launder & Sharma (1974) linear model and the Craft *et al.* (1996) cubic model. We replace the Reynolds stress constitutive relationship with (3.1), while retaining all other coefficients from these two models to ensure a fair comparison. In the following, we denote the new quadratic model based on the Launder & Sharma (1974) model as 'new model (1)' and the new quadratic model based on the Craft *et al.* (1996) model as 'new model (2)'.

To accurately capture the pronounced non-equilibrium effects in the shock-wave–boundary-layer interaction (SWBLI) cases, a specifically designed source term is introduced in the dissipation rate equation to control the excessive turbulent length scale in the SWBLI region. The source term is formulated as

$$S_{\varepsilon cm} = HY\lambda_l \frac{\tilde{\varepsilon}^2}{k}, \tag{3.4}$$

where the homogeneous dissipation rate $\tilde{\varepsilon}$ is defined as $\tilde{\varepsilon} = \varepsilon - 2\nu(\partial k^{1/2}/\partial x_j)^2$. Here, H is a calibration constant determined from numerical experiments, with recommended value 3. The term $\lambda_l = \max((k/\tilde{\varepsilon})(\partial u_k/\partial x_k), -0.5)$ is associated with velocity divergence, which vanishes in incompressible cases, and the coefficient -0.5 is introduced to maintain numerical stability. The switch function $Y = \tanh(2(\eta - 3)) - 1$ restricts the correction term to be primarily active in the near-wall viscous region, where $\eta = \max(\hat{S}, \hat{\Omega})$, with $\hat{S} = (k/\tilde{\varepsilon})\sqrt{2S_{ij}^d S_{ij}^d}$ and $\hat{\Omega} = (k/\tilde{\varepsilon})\sqrt{2\Omega_{ij}\Omega_{ij}}$. As demonstrated by Zhang *et al.* (2022), incorporating this source term significantly mitigates the severe overprediction of wall heat flux in the SWBLI region, while exerting only a limited influence on wall pressure distributions and flow separation. Consequently, the overall results remain in good agreement with experimental measurements. Notably, the magnitude of the correction is determined directly by the velocity divergence, thereby accounting for compressibility effects.

Although numerous compressibility corrections have been proposed, their effectiveness and general applicability remain open questions. Some researchers advocate incorporating these compressibility corrections into their turbulence models. For example, Wang & Fu (2011) and Fu & Wang (2013) integrated the dilatation–dissipation corrections proposed by Sarkar *et al.* (1991) and Sarkar (1995) into their $k-\omega-\gamma$ transition/turbulence model. This model has demonstrated remarkable success in engineering applications, and has been employed effectively to predict boundary layer transition in vehicles operating across a broad speed range, from subsonic to hypersonic. Conversely, some researchers suggest that incorporating these compressibility corrections is unnecessary for wall-bounded flows, as compressibility effects are generally not significant over a broad range of Mach numbers, and most turbulence models can already provide reasonably accurate predictions

https://doi.org/10.1017/jfm.2025.323 Published online by Cambridge University Press

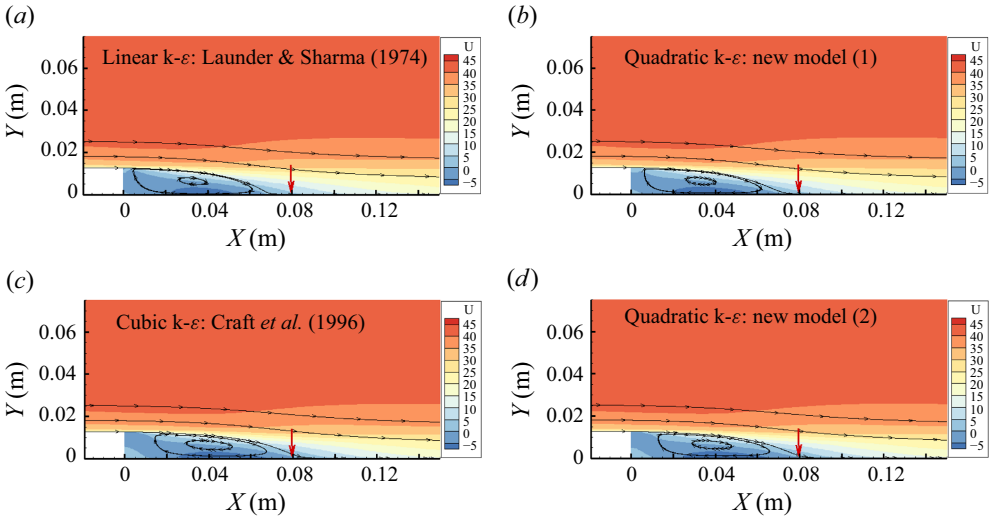


Figure 3. Two-dimensional backward-facing step: comparison of velocity contours and streamlines for the four models. The arrow represents the reattachment point measured in the experiment.

(So *et al.* 1998; Wilcox 1998; Rumsey 2010). Additionally, DNS results (Huang *et al.* 1995; Vreman *et al.* 1996; Li *et al.* 2022) indicate that the associated terms are small or negligible. Given the ongoing debate on this issue, these compressibility corrections are not adopted in this study.

3.2.1. *Two-dimensional backward-facing step*

The first case is based on the experiment by Driver & Seegmiller (1985), in which a series of laser Doppler velocimeter measurements were conducted for an incompressible turbulent flow over a backward-facing step in a diverging channel. Flow conditions upstream of the step were well developed, with a Reynolds number based on boundary layer momentum thickness 5000 at a location 4 step heights upstream of the step. The step height H is set as 1.27 cm, the expansion rate is 1 : 9/8, and the molecular viscosity is 1.5×10^{-5} m^2 s^{-1}. In our calculation, the inflow length has been adjusted so that the naturally developing turbulent boundary layer on the lower wall grows to approximately the correct thickness and yields approximately the correct wall skin friction coefficient prior to the step. The inflow velocity is adjusted to yield the correct Mach number ($Ma = 0.128$) upstream of the step. Calculations are performed on a rectilinear mesh of approximately 60 000 cells, ensuring that the $y+$ value at the wall is less than unity.

The reattachment length is a critical parameter for validating turbulence models in separated flow regions. We compare the reattachment lengths predicted by the four models with experimental measurements. As shown in figure 3, the Launder & Sharma (1974) model predicts a shorter separating length, while the Craft *et al.* (1996) model seems to overestimate it. The two new quadratic models developed in this work demonstrate improved accuracy. A quantitative comparison is presented in table 2. It is shown that by replacing the Reynolds stress with the expression in (3.1), the relative error of the reattachment length for the Launder & Sharma (1974) model decreases from 14.75 % to 6.27 %, and that of the Craft *et al.* (1996) model decreases from 9.63 % to 5.19 %.

https://doi.org/10.1017/jfm.2025.323 Published online by Cambridge University Press

Model	Reattachment length (x/H)	Relative error
Experiment	6.26 ± 0.1	–
Linear k-ε: Launder & Sharma (1974)	5.33	−14.75 %
Quadratic k-ε: new model (1)	5.86	−6.27 %
Cubic k-ε: Craft *et al.* (1996)	6.86	9.63 %
Quadratic k-ε: new model (2)	6.58	5.19 %

Table 2. Two-dimensional backward-facing step: comparison of reattachment length with the measured value for the four models.

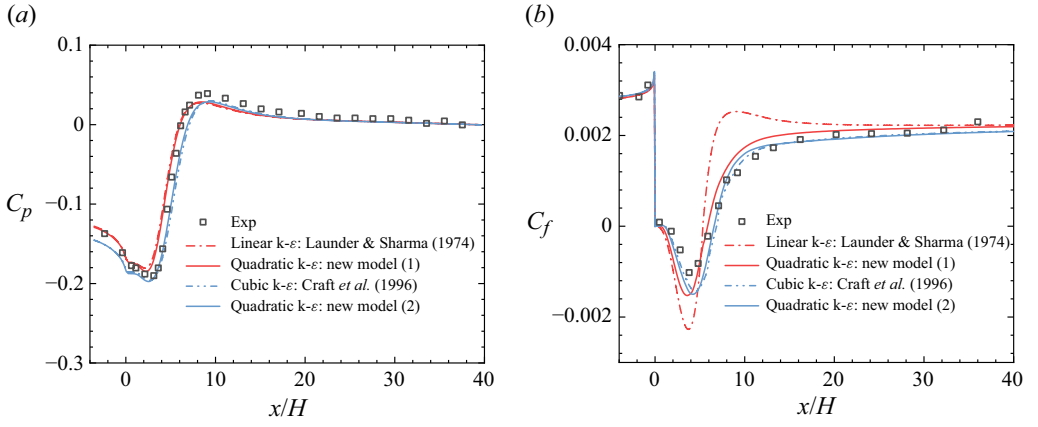


Figure 4. Two-dimensional backward-facing step: comparison of computed and measured surface pressure and skin friction coefficients downstream of the step for the four models.

Figure 4 compares the computed and measured surface pressure and skin friction coefficients downstream of the step. The pressure coefficients predicted by all four models are close to the experimental data. For the skin friction coefficients, the new model (1) demonstrates significant improvement over the original Launder & Sharma (1974) linear model, while the new model (2), though essentially quadratic, performs comparably to the cubic Craft *et al.* (1996) model. These results highlight the effectiveness of the Reynolds stress relation derived from the turbulent Fokker–Planck equation proposed in this work.

3.2.2. *Axisymmetric compression corner near $Ma = 7$*

The second case is based on the study by Kussoy & Horstman (1989), who investigated the flow over axisymmetric ogive-cylinder-flares at Mach number 7.05. The test model used in his experiment is shown in figure 5(*a*). He considered a flare angle of 35°, which represents a fully separated flow. The freestream temperature is 81.2 K, and the Reynolds number based on the nominal freestream conditions is 5,800,000 m^{-1}.

The set-up of our study is the same as that of Zhang *et al.* (2022). The computational grid, shown in figure 5(*b*), is a structured grid that is uniform in the streamwise direction and expands exponentially in the wall-normal direction. Both the cylinder and flare lengths are set to 20 cm, which is sufficient to cover the entire interaction region. The inlet boundary condition is determined by first calculating an undisturbed boundary layer flow over the cylinder and matching the measured and computed displacement thickness, which is 0.0074 m, at a point 6 cm upstream of the corner. A no-slip condition is applied to the

https://doi.org/10.1017/jfm.2025.323 Published online by Cambridge University Press

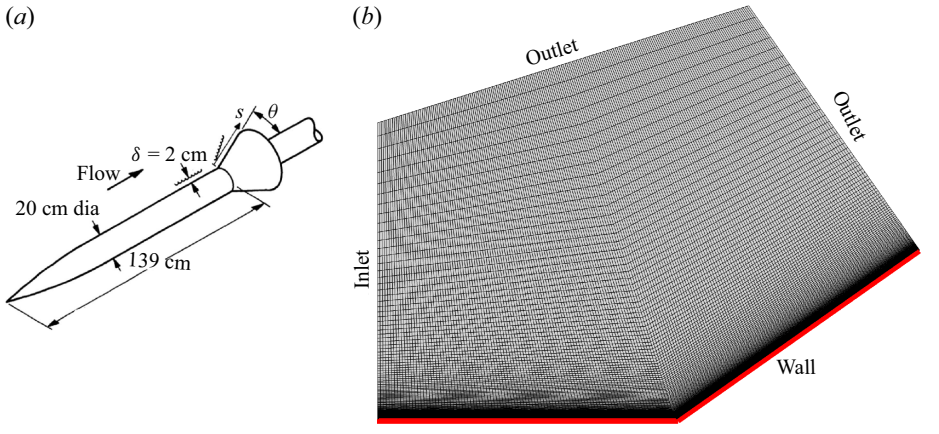


Figure 5. Axisymmetric compression corner: (*a*) the test model of the experiment of Kussoy & Horstman (1989); (*b*) computational grid for the compression corner case.

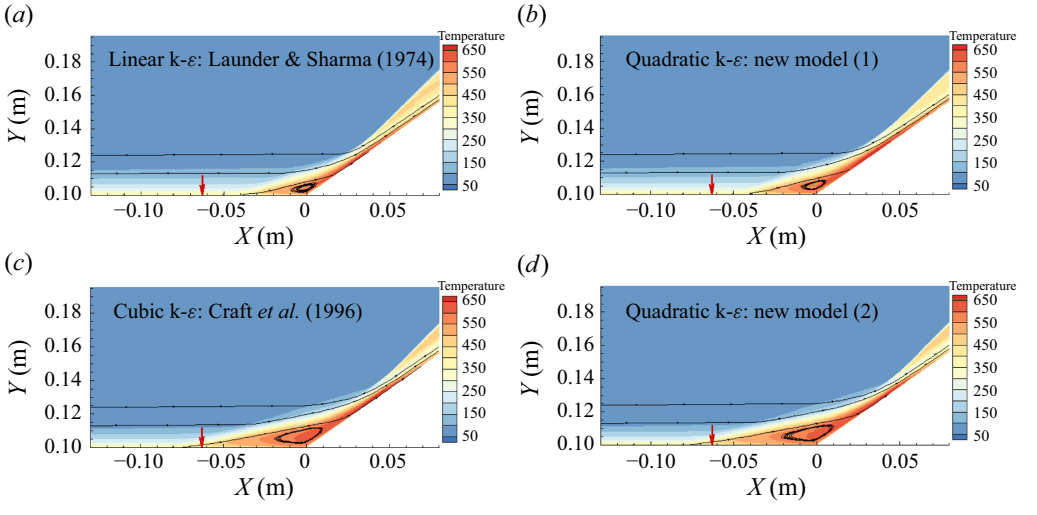


Figure 6. Axisymmetric compression corner: comparison of temperature contours and streamlines for the four models. The arrow represents the separating point measured in the experiment.

wall, with the wall temperature fixed at 311 K, and zero gradient for pressure. Zero-gradient conditions are also applied to all variables at the outlet boundaries. Since the test model is axisymmetric, the 'wedge' boundary condition of OpenFOAM is used to run axisymmetric simulations with one cell in the circumferential direction and angle 1°. The values of $y+$ at the first grid point off the wall are maintained below 0.1. A grid-independence test was conducted, showing that a mesh of 200×200 cells is sufficient to achieve numerically grid-independent results.

The temperature contours and streamlines predicted by the four models are shown in figure 6. The Launder & Sharma (1974) model and the new model (1) both predict a later separation, while the Craft *et al.* (1996) model and the new model (2) predict an earlier separation. For a quantitative comparison, as shown in figure 7, the surface pressure

https://doi.org/10.1017/jfm.2025.323 Published online by Cambridge University Press

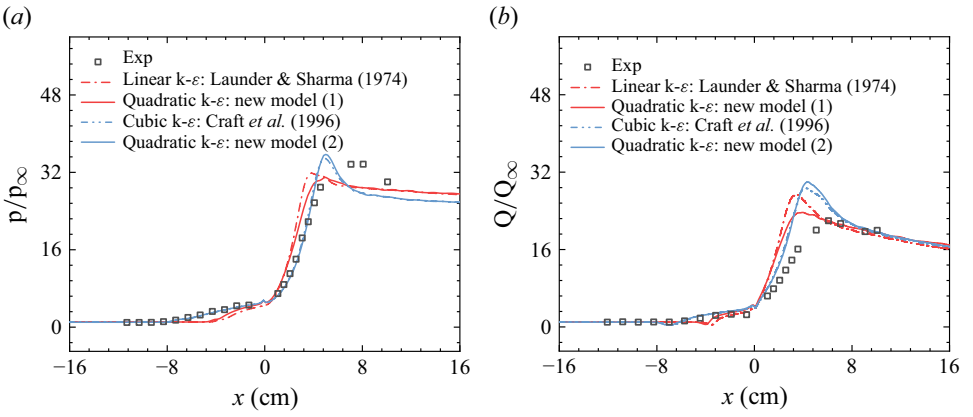


Figure 7. Axisymmetric compression corner: comparison of computed and measured surface pressure and heat flux at the wall for the four models.

and heat flux predicted by the new model (1) are closer to the experimental values than those predicted by the Launder & Sharma (1974) linear model. Specifically, the Launder & Sharma (1974) model overestimates the peak wall heat flux by approximately 24 %, while the new model (1) overestimates it by only 8 %. This aligns with the findings of Friedrich & Bertolotti (1996), who observed that compressibility effects enhance the anisotropy of the Reynolds stress due to turbulent fluctuations, and that NLEVMs provide a better foundation than linear models for improving predictions of compressibility effects. The results of the new model (2) are shown to be quite accurate and comparable to those of the cubic model, despite being only quadratic.

3.2.3. *Two-dimensional impinging shock near* $Ma = 8$

The third case is based on the experiment conducted by Kussoy & Horstman (1991), which involved a two-dimensional impinging shock generated by a shock generator with turning angle 10°. The test model is shown in figure 8(*a*). The free stream conditions are Mach number 8.18, pressure 430 Pa, temperature 81 K, and velocity 1446 m s^{-1}. In our calculation, the shock generator is included in the computational domain, as shown in figure 8(*b*). A structured grid with 570 × 180 cells is used to discretise the flow field. The grid points in the streamwise direction are clustered at the leading edge of the shock generator, uniformly distributed in the interaction region, and grow exponentially in the wall-normal direction. The inlet boundary conditions are set to ensure that the displacement thickness at a specified station, 47 cm behind the leading edge of the shock generator, matches the measured value, i.e. 1.59 cm. The inlet profiles are obtained from a separate calculation of undisturbed boundary layer flow on a flat plate. Zero-gradient conditions are applied to all variables at the outlet boundary. At the wall, a no-slip condition is applied, with the temperature fixed at the experimental value 300 K, and a zero-gradient condition for pressure.

The pressure contours and the separation bubbles predicted by the four models are presented in figure 9. The Launder & Sharma (1974) model and the new model (1) both predict a small separation bubble, while the Craft *et al.* (1996) model and the new model (2) predict a larger one. Figure 10 compares the computed surface pressure and heat flux at the wall with experimental measurements. It appears that higher-order terms play a minor role in this situation. The pressure profiles downstream of the interaction region are well predicted by all models, although the initial pressure rise predicted by the Launder &

https://doi.org/10.1017/jfm.2025.323 Published online by Cambridge University Press

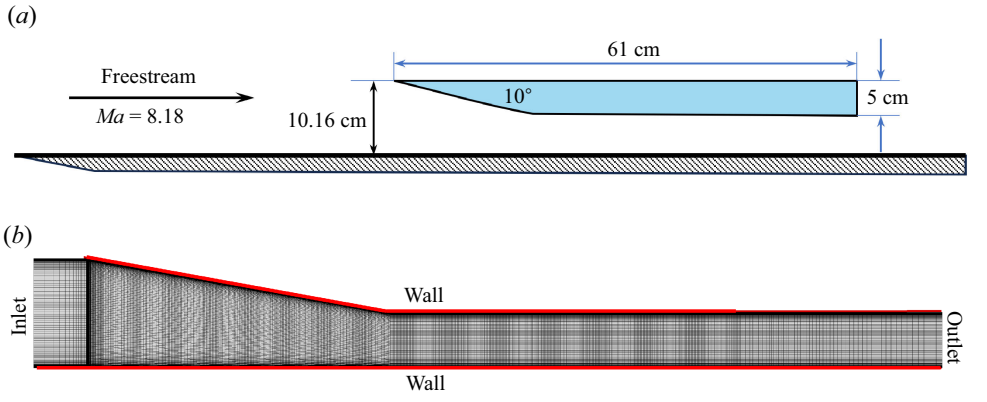


Figure 8. Two-dimensional impinging shock: (*a*) the test model of the experiment of Kussoy & Horstman (1991); (*b*) computational grid for the impinging shock case.

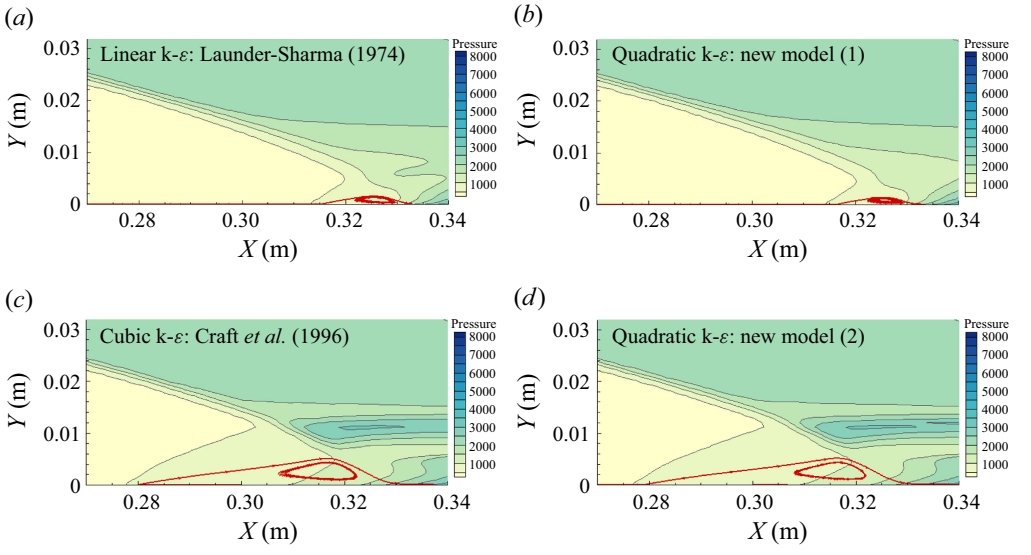


Figure 9. Two-dimensional impinging shock: comparison of pressure contours and separation bubbles for the four models.

Sharma (1974) model and the new model (1) is slightly underpredicted. The wall heat flux predicted by the Craft *et al.* (1996) model and the new model (2) fits the data very well, whereas the Launder & Sharma (1974) model and the new model (1) predict a slightly higher peak wall heat flux.

4. Conclusions and discussions

In this study, we proposed a Fokker–Planck equation for turbulence based on the analogy with molecules described by kinetic theory. This equation aims to characterise turbulent flows at the hydrodynamic level and can be viewed as a specific instance of Pope's GLM. We established a connection between the turbulent Fokker–Planck equation and the Reynolds stress constitutive relationship using the Chapman–Enskog expansion. When truncated to the zeroth order, the obtained solution corresponds to the isotropic part of the

https://doi.org/10.1017/jfm.2025.323 Published online by Cambridge University Press

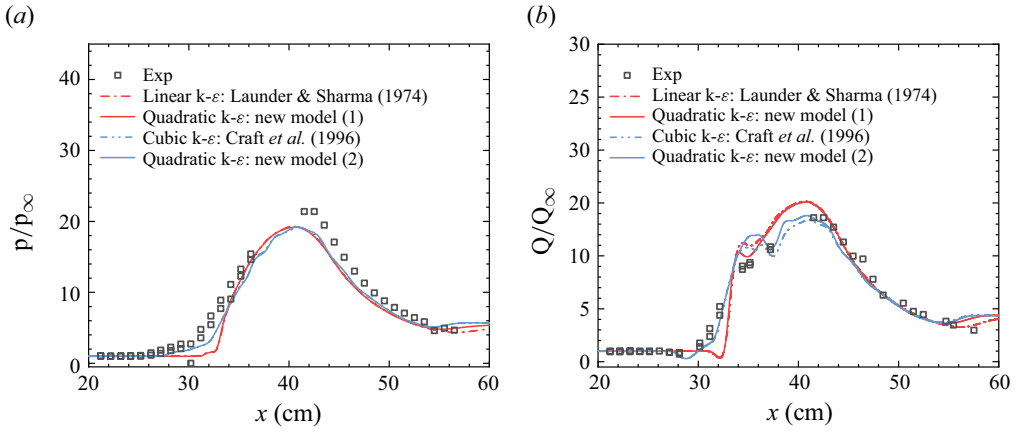


Figure 10. Two-dimensional impinging shock: comparison of computed and measured surface pressure and heat flux at the wall for the four models.

Reynolds stress. The first-order expansion yielded the well-known linear eddy viscosity model (EVM), while the second-order expansion resulted in a quadratic Reynolds stress constitutive relationship that also accounts for history effects.

We compared the coefficients of the quadratic Reynolds stress model with those of typical NLEVMs, and found them to be qualitatively consistent. Additionally, we implemented this quadratic Reynolds stress model in CFD codes and calculated three typical cases: a two-dimensional backward-facing step, an axisymmetric compression corner near Mach 7, and an impinging shock near Mach 8. The results indicate that the kinetic-based NLEVM developed in this work, without the use of *ad hoc* parameters in the Reynolds stress relationship, outperforms the traditional EVM and is comparable to a cubic model for two-dimensional flows.

Our efforts demonstrated the potential of deriving turbulence models from a kinetic perspective. Traditional models often struggle with the lack of scale separation between mean and fluctuating fields in the NS equations when incorporating eddy viscosity. In contrast, kinetic theory does not rely on scale separation, offering a distinct advantage in turbulence modelling. We demonstrated that turbulence models can be effectively encapsulated within a kinetic equation for turbulence. Compared to the similar work conducted by Chen *et al.* (2003, 2004), which treats turbulent motion as a BGK-type relaxation process, describing turbulent motion as a stochastic process governed by a Fokker–Planck equation appears to be a more suitable approach. In this study, we expanded the turbulent Fokker–Planck equation to second order. As noted by Launder (1996), the introduction of nonlinear terms at the quadratic level proved insufficient for accurately capturing the effects of streamline curvature and the behaviour of three-dimensional flows. Notably, the same methodology can be used to perform higher-order expansions, generating additional terms to further refine the model.

As highlighted in § 2.1, there are two fundamentally different approaches to deriving turbulence models from kinetic theory. The approach adopted in this study involves first establishing a coarse-grained kinetic equation at the hydrodynamic level, then applying the Chapman–Enskog expansion to derive the constitutive relationship between Reynolds stress and average flow variables. The key challenge in this method lies in constructing the coarse-grained kinetic equation. In this study, we address this challenge by drawing an analogy between turbulent dynamics and Brownian motion. A more rigorous approach,

https://doi.org/10.1017/jfm.2025.323 Published online by Cambridge University Press

such as directly coarse-graining the kinetic equation for molecules, remains a challenging yet promising area for future research.

Acknowledgements. The authors would like to thank Xiaoyong Wang and Jinglei Xu for valuable suggestions. The authors would also like to thank Xinliang Li and Ji Zhang for many helpful discussions.

Funding. This work was supported by the National Natural Science Foundation of China (grant nos 92371102 and 12272028).

Declaration of interests. The authors report no conflict of interest.

Appendix A. Moments of the Fokker–Planck equation for turbulence

From the Fokker–Planck equation for turbulence, i.e. (2.6), the corresponding moment equations can be straightforwardly derived.

We firstly multiply both sides of (2.6) by a generalised property function Q, which is a function of the particle velocity and is therefore independent of space and time. Then integrating the product over the entire velocity space yields the extended moment equation

$$\frac{\partial(n\bar{Q})}{\partial t}+\frac{\partial(n\overline{Qu_k})}{\partial x_k}-n\frac{1}{\rho}\frac{\partial\sigma_{ij}}{\partial x_j}\frac{\partial\bar{Q}}{\partial u_i}=\Delta\left[Q\right]. \tag{A1}$$

In (A1), the source term $\Delta[Q]$ is defined as

$$\Delta\left[Q\right]=\int_{R^3}Q\left(\frac{1}{\tau_T}\frac{\partial}{\partial u_k}[f(u_k-\bar{u}_k)]+\frac{2k}{3\tau_T}\frac{\partial^2 f}{\partial u_k\,\partial u_k}\right)\mathrm{d}\boldsymbol{u}. \tag{A2}$$

If Q is taken as mass m and fluid particle velocity u_i, respectively, then the source terms vanish and the RANS equations at the average flow field level are recovered, i.e.

$$\begin{cases}\dfrac{\partial\rho}{\partial t}+\dfrac{\partial\rho\bar{u}_j}{\partial x_j}=0,\\[2ex] \dfrac{\partial\bar{u}_i}{\partial t}+\bar{u}_j\dfrac{\partial\bar{u}_i}{\partial x_j}-\dfrac{1}{\rho}\dfrac{\partial\sigma_{ij}}{\partial x_j}-\dfrac{1}{\rho}\dfrac{\partial\sigma_{ij}^T}{\partial x_j}=0.\end{cases} \tag{A3}$$

In (A3), $\sigma_{ij}^T=-\overline{\rho u_i' u_j'}$ is the Reynolds stress.

If Q is taken as u_iu_j, and we simplify the resulting equation using (A3), then a partially modelled Reynolds stress transport equation can be obtained:

$$\frac{D\overline{u_i'u_j'}}{Dt}+\frac{\partial\overline{u_i'u_j'u_k'}}{\partial x_k}=P_{ij}+\frac{1}{\rho}\frac{\partial\sigma_{mn}}{\partial x_n}\frac{\partial\overline{u_i'u_j'}}{\partial u_m}-\frac{2}{\tau_T}\overline{u_i'u_j'}+\frac{4}{3}\frac{k}{\tau_T}\delta_{ij}. \tag{A4}$$

The first three terms, representing mean convection, turbulent transport and production, are exact. When comparing (A4) with the exact Reynolds stress transport equation, and neglecting the viscous and pressure transport terms, the corresponding redistribution and dissipation terms are modelled as

$$R_{ij}-\varepsilon_{ij}=\frac{1}{\rho}\frac{\partial\sigma_{mn}}{\partial x_n}\frac{\partial\overline{u_i'u_j'}}{\partial u_m}-\frac{2}{\tau_T}\overline{u_i'u_j'}+\frac{4}{3}\frac{k}{\tau_T}\delta_{ij}. \tag{A5}$$

https://doi.org/10.1017/jfm.2025.323 Published online by Cambridge University Press

Taking dissipation to be isotropic, the pressure rate of strain model implied by the Fokker–Planck equation for turbulence is

$$R_{ij} = \frac{1}{\rho}\frac{\partial \sigma_{mn}}{\partial x_n}\frac{\partial \overline{u_i' u_j'}}{\partial u_m} - \frac{2}{\tau_T}\overline{u_i' u_j'} + \left(\frac{4}{3}\frac{k}{\tau_T} + \frac{2}{3}\varepsilon\right)\delta_{ij}. \tag{A6}$$

The requirement that R_{ij} be redistributive (i.e. $R_{ii} = 0$) leads to the dissipation rate as

$$\varepsilon = -\frac{1}{\rho}\frac{\partial \sigma_{mn}}{\partial x_n}\frac{\partial k}{\partial u_m}, \tag{A7}$$

which indicates that the dissipation of turbulent kinetic energy is related to molecular viscosity.

Appendix B. The eigenfunctions of the Fokker–Planck operator

The Fokker–Planck operator, defined as

$$L[Q] = \frac{1}{f_M}\frac{\partial}{\partial u_i}\left[\frac{2}{3}k\, f_M \frac{\partial}{\partial u_i}(Q)\right], \tag{B1}$$

is a linear operator. Its eigenfunctions, denoted by Q, possess the property

$$L[Q] = \lambda Q, \tag{B2}$$

where λ are the corresponding eigenvalues. To obtain solutions for the Chapman–Enskog expansion of the Fokker–Planck model, we identify several eigenfunctions as follows:

$$A_{ij} = u_i' u_j' - \frac{1}{3}u_k' u_k' \delta_{ij}, \tag{B3}$$

$$B_j = u_j'\left(\frac{\boldsymbol{u}'^2}{2} - \frac{5}{2}\frac{2}{3}k\right), \tag{B4}$$

$$Q_{E_1} = u_i'\frac{\partial S_{ij}^d}{\partial x_j}, \tag{B5}$$

$$Q_{E_2} = \frac{u_i' u_i'}{4k/3} - \frac{3}{2}, \tag{B6}$$

$$Q_A = \left(u_i' u_j'\frac{\partial \bar{u}_i}{\partial x_j} - \frac{1}{3}u_m' u_m'\frac{\partial \bar{u}_i}{\partial x_j}\delta_{ij}\right)^2, \tag{B7}$$

$$Q_{B_1} = u_i' u_j' - \frac{1}{3}u_k' u_k' \delta_{ij}, \tag{B8}$$

$$Q_{B_2} = u_l'\frac{\partial}{\partial x_l}\left(\frac{\partial \bar{u}_i}{\partial x_j}\right)\left(u_i' u_j' - \frac{1}{3}u_k' u_k' \delta_{ij}\right), \tag{B9}$$

$$Q_C = \left(u_l' u_j'\frac{\partial \bar{u}_i}{\partial x_l} + u_l' u_i'\frac{\partial \bar{u}_j}{\partial x_l} - \frac{2}{3}u_k' u_l'\frac{\partial \bar{u}_k}{\partial x_l}\delta_{ij}\right)\frac{\partial \bar{u}_i}{\partial x_j}, \tag{B10}$$

$$Q_{D_1} = \frac{1}{\rho}\frac{\partial \sigma_{lj}}{\partial x_j}u_l'\left(u_i' u_j' - \frac{1}{3}u_k' u_k' \delta_{ij}\right)\frac{\partial \bar{u}_i}{\partial x_j}, \tag{B11}$$

https://doi.org/10.1017/jfm.2025.323 Published online by Cambridge University Press

$$Q_{D_2} = \frac{1}{\rho}\frac{\partial \sigma_{lj}}{\partial x_j}\left(u'_j\frac{\partial \bar{u}_l}{\partial x_j} + u'_i\frac{\partial \bar{u}_i}{\partial x_l} - \frac{2}{3}u'_l\delta_{ij}\frac{\partial \bar{u}_i}{\partial x_j}\right), \tag{B12}$$

$$D = \frac{\partial}{\partial x_j}\left(\frac{\partial \bar{u}_i}{\partial x_j}\right)u'_i + \frac{\partial}{\partial x_i}\left(\frac{\partial \bar{u}_i}{\partial x_j}\right)u'_j - \frac{2}{3}\frac{\partial}{\partial x_m}\left(\frac{\partial \bar{u}_i}{\partial x_j}\right)u'_m\delta_{ij}, \tag{B13}$$

$$\begin{aligned} M = {} & u'_i u'_s \frac{\partial \bar{u}_i}{\partial x_m}\frac{\partial \bar{u}_s}{\partial x_m} + u'_j u'_s \frac{\partial \bar{u}_m}{\partial x_j}\frac{\partial \bar{u}_s}{\partial x_m} - \frac{2}{3}u'_m u'_s \frac{\partial \bar{u}_n}{\partial x_n}\frac{\partial \bar{u}_s}{\partial x_m} \\ & + u'_i u'_t \frac{\partial \bar{u}_i}{\partial x_m}\frac{\partial \bar{u}_m}{\partial x_t} + u'_j u'_t \frac{\partial \bar{u}_m}{\partial x_j}\frac{\partial \bar{u}_m}{\partial x_t} - \frac{2}{3}u'_m u'_t \frac{\partial \bar{u}_n}{\partial x_n}\frac{\partial \bar{u}_m}{\partial x_t} \\ & - \frac{2}{3}u'_i u'_m \frac{\partial \bar{u}_i}{\partial x_m}\frac{\partial \bar{u}_n}{\partial x_n} - \frac{2}{3}u'_j u'_m \frac{\partial \bar{u}_m}{\partial x_j}\frac{\partial \bar{u}_n}{\partial x_n} + \frac{4}{9}u'_k u'_k \frac{\partial \bar{u}_m}{\partial x_m}\frac{\partial \bar{u}_n}{\partial x_n}, \end{aligned} \tag{B14}$$

$$N = \frac{\partial \bar{u}_k}{\partial x_m}\frac{\partial \bar{u}_k}{\partial x_m} + \frac{\partial \bar{u}_k}{\partial x_m}\frac{\partial \bar{u}_m}{\partial x_k} - \frac{2}{3}\frac{\partial \bar{u}_m}{\partial x_m}\frac{\partial \bar{u}_k}{\partial x_k}. \tag{B15}$$

It is straightforward to demonstrate that

$$\begin{aligned} L\left[A_{ij}\right] &= -2A_{ij}, \\ L\left[B_j\right] &= -3B_j, \\ L\left[Q_{E_1}\right] &= -Q_{E_1}, \\ L\left[Q_{E_2}\right] &= -2Q_{E_2}, \\ L\left[Q_A\right] &= -4Q_A + 2\theta M, \\ L\left[Q_{B_1}\right] &= -2Q_{B_1}, \\ L\left[Q_{B_2}\right] &= -3Q_{B_2} + 2\theta D, \\ L\left[Q_C\right] &= -2Q_C + 2\theta N, \\ L\left[Q_{D_1}\right] &= -3Q_{D_1} + \tfrac{4}{3}kQ_{D_2}, \\ L\left[Q_{D_2}\right] &= -3Q_{D_2}, \\ L\left[D\right] &= -D, \\ L\left[M\right] &= -2M + 4\theta N, \\ L\left[N\right] &= 0. \end{aligned} \tag{B16}$$

By using these eigenfunctions, we can expand the distribution function in terms of the eigenfunctions of the Fokker–Planck operator, and obtain the coefficients through the Chapman–Enskog expansion.

Appendix C. The integrals of $f^{(2)}$ correspond to the Fokker–Planck equation for turbulence

The second-order expansion of the turbulent Fokker–Planck equation is expressed in (2.50). To derive the Reynolds stress up to second order, we integrate $mu'_{\langle i}u'_{j\rangle}$ with respect

https://doi.org/10.1017/jfm.2025.323 Published online by Cambridge University Press

to the second-order distribution function $f^{(2)}$, handling each component term by term, and then reformulate the results into tensorial form. The relevant integrals are computed and presented as follows:

$$\int_{R^3} mu'_{\langle i}u'_{j\rangle} f_M \left[-\frac{4}{3}k\, Q_{E_1}\right] \mathrm{d}\boldsymbol{u}' = 0, \tag{C1}$$

$$\int_{R^3} mu'_{\langle i}u'_{j\rangle} f_M \left[-\frac{4}{9}k\, S^d_{ij}\frac{\partial \bar{u}_i}{\partial x_j}\, Q_{E_2}\right] \mathrm{d}\boldsymbol{u}' = 0, \tag{C2}$$

$$\int_{R^3} mu'_{\langle i}u'_{j\rangle} f_M \left[\frac{1}{8k/3}\, Q_A\right] \mathrm{d}\boldsymbol{u}' = \frac{1}{2}\rho\left(\frac{2}{3}k\right)^2 \times \left[4\left(S_{ik}S_{kj} - \frac{2}{3}S_{ij}S_{mm}\right) - \frac{4}{3}\left(S_{mn}S_{mn} - \frac{2}{3}S_{mm}S_{nn}\right)\delta_{ij}\right], \tag{C3}$$

$$\int_{R^3} mu'_{\langle i}u'_{j\rangle} f_M \frac{1}{2}\left[\frac{\partial_0}{\partial t}\left(\frac{\partial \bar{u}_i}{\partial x_j}\right) + \bar{u}_l\frac{\partial}{\partial x_l}\left(\frac{\partial \bar{u}_i}{\partial x_j}\right)\right] Q_{B_1}\mathrm{d}\boldsymbol{u}' = \rho\left(\frac{2}{3}k\right)^2\left(\frac{\partial_0}{\partial t} + \bar{u}_l\frac{\partial}{\partial x_l}\right) S^d_{ij}, \tag{C4}$$

$$\int_{R^3} mu'_{\langle i}u'_{j\rangle} f_M \left[\frac{1}{3}\, Q_{B_2}\right] \mathrm{d}\boldsymbol{u}' = 0, \tag{C5}$$

$$\int_{R^3} mu'_{\langle i}u'_{j\rangle} f_M \left[-\frac{1}{2}\, Q_C\right] \mathrm{d}\boldsymbol{u}' = -\rho\left(\frac{2}{3}k\right)^2 \times \left[S_{ik}\frac{\partial \bar{u}_k}{\partial x_j} + S_{jk}\frac{\partial \bar{u}_k}{\partial x_i} - \frac{2}{3}S_{ij}S_{mm} - \frac{2}{3}\left(S_{mn}S_{mn} - \frac{1}{3}S_{mm}S_{nn}\right)\delta_{ij}\right], \tag{C6}$$

$$\int_{R^3} mu'_{\langle i}u'_{j\rangle} f_M \left[\frac{4}{9}k\, Q_{D_1}\right] \mathrm{d}\boldsymbol{u}' = 0, \tag{C7}$$

$$\int_{R^3} mu'_{\langle i}u'_{j\rangle} f_M \left[\frac{4}{9}k\, Q_{D_2}\right] \mathrm{d}\boldsymbol{u}' = 0, \tag{C8}$$

$$\int_{R^3} mu'_{\langle i}u'_{j\rangle} f_M \left[\frac{4}{9}k\, D\right] \mathrm{d}\boldsymbol{u}' = 0, \tag{C9}$$

$$\int_{R^3} mu'_{\langle i}u'_{j\rangle} f_M \left[\frac{1}{4}\, M\right] \mathrm{d}\boldsymbol{u}' = 2\rho\left(\frac{2}{3}k\right)^2 \times \left[\left(S_{ik}S_{kj} - \frac{2}{3}S_{ij}S_{mm}\right)\right] - \frac{1}{3}\left(S_{mn}S_{mn} - \frac{2}{3}S_{mm}S_{nn}\right)\delta_{ij}. \tag{C10}$$

The expressions for eigenfunctions such as Q_{E_1}, Q_{E_2} and others are given in Appendix B. Summarising these integrals, we obtain the second-order Reynolds stress. After reorganisation, the result can be expressed as

$$\sigma^{T(2)}_{ij} = -\frac{1}{2}\rho\tau_T^2\left(\frac{2}{3}k\right)\left(\frac{\partial_0}{\partial t} + \bar{u}_k\frac{\partial}{\partial x_k}\right) S^d_{ij} - \rho\tau_T^2\left(\frac{2}{3}k\right)\left(S^d_{ik}S^d_{kj} - \frac{1}{3}S^d_{mn}S^d_{mn}\delta_{ij}\right) + \frac{1}{2}\rho\tau_T^2\left(\frac{2}{3}k\right)(S^d_{ik}\Omega_{kj} + S^d_{jk}\Omega_{ki}). \tag{C11}$$

https://doi.org/10.1017/jfm.2025.323 Published online by Cambridge University Press

References

Apsley, D.D. & Leschziner, M.A. 1998 A new low-Reynolds-number nonlinear two-equation turbulence model for complex flows. *Intl J. Heat Fluid Flow* **19** (3), 209–222.

Boussinesq, J. 1870 Essai théorique sur les lois trouvées expérimentalement par M. Bazin pour l'écoulement uniforme de l'eau dans les canaux découverts. *C. R. Acad. Sci. Paris* **71**, 389–393.

Cercignani, C. 1988 *The Boltzmann Equation*. Springer.

Chapman, S. & Cowling, T.G. 1990 *The Mathematical Theory of Non-Uniform Gases: An Account of the Kinetic Theory of Viscosity, Thermal Conduction and Diffusion in Gases*. Cambridge University Press.

Chen, H., Kandasamy, S., Orszag, S., Shock, R., Succi, S. & Yakhot, V. 2003 Extended Boltzmann kinetic equation for turbulent flows. *Science* **301** (5633), 633–636.

Chen, H., Orszag, S.A., Staroselsky, I. & Succi, S. 2004 Expanded analogy between Boltzmann kinetic theory of fluids and turbulence. *J. Fluid Mech.* **519**, 301–314.

Chen, H., Staroselsky, I., Sreenivasan, K. R., & Yakhot, V. 2023 Average turbulence dynamics from a one-parameter kinetic theory. *Atmosphere* **14** (7), 1109.

Chen, H., Staroselsky, I., Sreenivasan, K.R., & Yakhot, V. 2024 Average turbulence dynamics from a one-parameter kinetic theory: Estimation of the relaxation time. *Phys. Fluids* **36** (3), 035156.

Chong, K.L., Shi, J.-Q., Ding, G.-Y., Ding, S.-S., Lu, H.-Y., Zhong, J.-Q. & Xia, K.-Q. 2020 Vortices as Brownian particles in turbulent flows. *Sci. Adv.* **6** (34), eaaz1110.

Chung, P.M. 1969 A simplified statistical model of turbulent, chemically reacting shear flows. *AIAA J.* **7** (10), 1982–1991.

Craft, T., Launder, B. & Suga, K. 1996 Development and application of a cubic eddy-viscosity model of turbulence. *Intl J. Heat Fluid Flow* **17** (2), 108–115.

Driver, D.M. & Seegmiller, H. 1985 Features of a reattaching turbulent shear layer in divergent channelflow. *AIAA J.* **23** (2), 163–171.

Durbin, P.A. 2018 Some recent developments in turbulence closure modeling. *Annu. Rev. Fluid Mech.* **50** (1), 77–103.

Friedrich, R. & Bertolotti, F. 1996 Compressibility effects due to turbulent fluctuations. *Appl. Sci. Res.* **57** (3–4), 165–194.

Fu, S., Guo, Y., Qian, W. & Wang, C. 2003 Recent progress in nonlinear eddy-viscosity turbulence modeling. *Acta Mechanica Sin.* **19** (5), 409–419.

Fu, S. & Pope, S. 1994 Computation of recirculating swirling flow with the GLM Reynolds stress closure. *Acta Mechanica Sin.* **10** (2), 110–120.

Fu, S., Wang, C. & Guo, Y. 2011 On the minimal representation of non-linear eddy-viscosity models. *J. Turbul.* **12**, N47.

Fu, S., Wang, C., Rung, T. & Thiele, F. 1997 Validation of the realizable quadratic eddy-viscosity model in turbulent secondary flow. In *International Symposium on Computational Fluid Dynamics*, pp. 429–434. International Academic.

Fu, S. & Wang, L. 2013 RANS modeling of high-speed aerodynamic flow transition with consideration of stability theory. *Prog. Aerosp. Sci.* **58**, 36–59.

Gallis, M., Bitter, N., Koehler, T., Torczynski, J., Plimpton, S. & Papadakis, G. 2017 Molecular-level simulations of turbulence and its decay. *Phys. Rev. Lett.* **118** (6), 064501.

Gatski, T.B. & Speziale, C.G. 1993 On explicit algebraic stress models for complex turbulent flows. *J. Fluid Mech.* **254**, 59–78.

Girimaji, S.S. 2007 Boltzmann kinetic equation for filtered fluid turbulence. *Phys. Rev. Lett.* **99** (3), 034501.

Greenshields, C.J., Weller, H.G., Gasparini, L. & Reese, J.M. 2010 Implementation of semi-discrete, non-staggered central schemes in a colocated, polyhedral, finite volume framework, for high-speed viscous flows. *Intl J. Numer. Meth. Fluids* **63** (1), 1–21.

Hanjalić, K. 1994 Advanced turbulence closure models: a view of current status and future prospects. *Intl J. Heat Fluid Flow* **15** (3), 178–203.

Haworth, D.C. & Pope, S.B. 1986 A generalized Langevin model for turbulent flows. *Phys. Fluids* **29** (2), 387–405.

Haworth, D.C. & Pope, S.B. 1987 A pdf modeling study of self-similar turbulent free shear flows. *Phys. Fluids* **30** (4), 1026–1044.

Heinz, S. 2003 *Statistical Mechanics of Turbulent Flows*. Springer.

Heinz, S. 2004 Molecular to fluid dynamics: the consequences of stochastic molecular motion. *Phys. Rev.* E: *Stat. Nonlinear Soft Matt. Phys.* **70** (3), 036308.

Heinz, S. 2007 Unified turbulence models for LES and RANS, FDF and PDF simulations. *Theor. Comp. Fluid Dyn.* **21** (2), 99–118.

https://doi.org/10.1017/jfm.2025.323 Published online by Cambridge University Press

HUANG, P.G., COLEMAN, G.N. & BRADSHAW, P. 1995 Compressible turbulent channel flows: DNS results and modelling. *J. Fluid Mech.* **305**, 185–218.

JASAK, H. JEMCOV, A., & TUKOVIĆ, Z. 2007 Openfoam: a C++ library for complex physics simulations. In *Proceedings of the International Workshop on Coupled Methods in Numerical Dynamics*. str. 47–66. Fakultet strojarstva i brodogradnje Sveučilišta u Zagrebu.

JENNY, P., TORRILHON, M. & HEINZ, S. 2010 A solution algorithm for the fluid dynamic equations based on a stochastic model for molecular motion. *J. Comput. Phys.* **229** (4), 1077–1098.

KIM, K.H., KIM, C. & RHO, O.-H. 2001 Methods for the accurate computations of hypersonic flows: I. AUSMPW+ scheme. *J. Comput. Phys.* **174** (1), 38–80.

KIRKWOOD, J.G. 1946 The statistical mechanical theory of transport processes I. General theory. *J. Chem. Phys.* **14** (3), 180–201.

KIRKWOOD, J.G., BUFF, F.P. & GREEN, M.S. 1949 The statistical mechanical theory of transport processes. III. The coefficients of shear and bulk viscosity of liquids. *J. Chem. Phys.* **17** (10), 988–994.

KOLMOGOROV, A.N. 1962 A refinement of previous hypotheses concerning the local structure of turbulence in a viscous incompressible fluid at high Reynolds number. *J. Fluid Mech.* **13** (1), 82–85.

KUSSOY, M.I. & HORSTMAN, C.C. 1989 Documentation of two- and three-dimensional hypersonic shock wave/turbulent boundary layer interaction flows. No. NASA-TM-101075. NASA Ames Research Center.

KUSSOY, M.I. & HORSTMAN, K. 1991 *Documentation of Two- and Three-Dimensional Shock-Wave/Turbulent-Boundary-Layer Interaction Flows at Mach 8.2*. NASA Ames Research Center Technical Report.

LANGEVIN, P. 1908 On the theory of Brownian motion. *C. R. Acad Sci. Paris* **146**, 530.

LAUNDER, B.E. 1996 An introduction to single-point closure methodology. In *Simulation and Modeling of Turbulent Flows* (ed. T.B Gatski, M. Hussaini & J.L Lumley), online edn. Oxford Academic.

LAUNDER, B.E., REECE, G.J. & RODI, W. 1975 Progress in the development of a Reynolds-stress turbulence closure. *J. Fluid Mech.* **68** (3), 537–566.

LAUNDER, B.E. & SHARMA, B.I. 1974 Application of the energy-dissipation model of turbulence to the calculation of flow near a spinning disc. *Lett. Heat Mass Transfer* **1** (2), 131–137.

LAUNDER, B.E. & SPALDING, D.B. 1983 The numerical computation of turbulent flows. In *Numerical Prediction of Flow, Heat Transfer, Turbulence and Combustion*, pp. 96–116. Elsevier.

LI, D., KOMPERDA, J., PEYVAN, A., GHIASI, Z. & MASHAYEK, F. 2022 Assessment of turbulence models using DNS data of compressible plane free shear layer flow. *J. Fluid Mech.* **931**, A10.

MALASPINAS, O. & SAGAUT, P. 2012 Consistent subgrid scale modelling for lattice Boltzmann methods. *J. Fluid Mech.* **700**, 514–542.

MCMULLEN, R.M., KRYGIER, M.C., TORCZYNSKI, J.R. & GALLIS, M.A. 2022 Navier–Stokes equations do not describe the smallest scales of turbulence in gases. *Phys. Rev. Lett.* **128** (11), 114501.

MENTER, F. 1997 Eddy viscosity transport equations and their relation to the k-ε model. *J. Fluids Engng* **119** (4), 876–884.

MISHRA, A. & GIRIMAJI, S. 2016 Manufactured turbulence with Langevin equations. arXiv preprint arXiv: 1611.03834.

MOIN, P. & MAHESH, K. 1998 Direct numerical simulation: a tool in turbulence research. *Annu. Rev. Fluid Mech.* **30** (1), 539–578.

MONIN, A.S. & YAGLOM, A.M. 2013 Statistical fluid mechanics. In *Mechanics of Turbulence*, vol. **2**. Courier Corporation.

MYONG, H.K. & KASAGI, N. 1990 A new approach to the improvement of k-ε turbulence model for wall-bounded shear flows. *JSME Intl J. 2* **33** (1), 63–72.

NISIZIMA, S. & YOSHIZAWA, A. 1987 Turbulent channel and Couette flows using an anisotropic k-epsilon model. *AIAA J.* **25** (3), 414–420.

POPE, S.B. 1975 A more general effective-viscosity hypothesis. *J. Fluid Mech.* **72** (2), 331–340.

POPE, S.B. 1985 PDF methods for turbulent reactive flows. *Prog. Energy Combust.* **11** (2), 119–192.

POPE, S.B. 2001 Turbulent flows. *Meas. Sci. Technol.* **12** (11), 2020–2021.

PRANDTL, L. 1925 7. Bericht über untersuchungen zur ausgebildeten turbulenz. *J. Appl. Maths Mech.* **5** (2), 136–139.

REYNOLDS, O. 1895 IV. On the dynamical theory of incompressible viscous fluids and the determination of the criterion. *Phil. Trans. R. Soc. Lond. A* **186**, 123–164.

RIGHI, M. 2016 A gas-kinetic scheme for turbulent flow. *Flow Turbul. Combust.* **97** (1), 121–139.

ROTTA, J.C. 1951 Statistische theorie nichthomogener turbulenz. *Zeitschrift für Physik* **129** (6), 547–572.

RUBINSTEIN, R. & BARTON, J.M. 1990 Nonlinear Reynolds stress models and the renormalization group. *Phys. Fluids A: Fluid Dyn.* **2** (8), 1472–1476.

https://doi.org/10.1017/jfm.2025.323 Published online by Cambridge University Press

RUMSEY, C.L. 2010 Compressibility considerations for k-ω turbulence models in hypersonic boundary-layer applications. *J. Spacecr. Rockets* **47** (1), 11–20.

RUNG, T., THIELE, F. & FU, S. 1998 On the realizability of nonlinear stress–strain relationships for Reynolds stress closures. *Flow Turbul. Combust.* **60** (4), 333–359.

SAMIEE, M., AKHAVAN-SAFAEI, A. & ZAYERNOURI, M. 2020 A fractional subgrid-scale model for turbulent flows: Theoretical formulation and *a priori* study. *Phys. Fluids* **32** (5), 055102.

SARKAR, S. 1995 The stabilizing effect of compressibility in turbulent shear flow. *J. Fluid Mech.* **282**, 163–186.

SARKAR, S., ERLEBACHER, G., HUSSAINI, M.Y. & KREISS, H.O. 1991 The analysis and modelling of dilatational terms in compressible turbulence. *J. Fluid Mech.* **227**, 473–493.

SHIH, T.-H., ZHU, J. & LUMLEY, J.L. 1993 *A realizable Reynolds stress algebraic equation model. Symposium on turbulence shear flows*. No. CMOTT-92-14. National Aeronautics and Space Administration.

SINGH, S.K. & ANSUMALI, S. 2015 Fokker–Planck model of hydrodynamics. *Phys. Rev.* E **91** (3), 033303.

SO, R.M.C., GATSKI, T.B. & SOMMER, T.P. 1998 Morkovin hypothesis and the modeling of wall-bounded compressible turbulent flows. *AIAA J.* **36** (9), 1583–1592.

SPALART, P. & ALLMARAS, S. 1992 A one-equation turbulence model for aerodynamic flows. In *30th Aerospace Sciences Meeting and Exhibit*, 06 January 1992 - 09 January 1992 Reno, NV, U.S.A., pp. 439. https://doi.org/10.2514/6.1992-439

SPEZIALE, C.G. 1987 On nonlinear K-l and K-ε models of turbulence. *J. Fluid Mech.* **178**, 459–475.

SUCCI, S. 2020 Towards a self-consistent Boltzmann's kinetic model of fluid turbulence. *J. Turbul.* **21** (7), 375–385.

TAVOULARIS, S. & CORRSIN, S. 1981 Experiments in nearly homogenous turbulent shear flow with a uniform mean temperature gradient. Part 1. *J. Fluid Mech.* **104**, 311–347.

TAYLOR, G.I. 1935 Statistical theory of turbulence. *Proc. R. Soc. Lond. A: Math. Phys. Sci.* **151** (873), 421–444.

THOMSON, W. 1887 XLV. On the propagation of laminar motion through a turbulently moving inviscid liquid. *Lond. Edinburgh Dublin Phil. Mag. J. Sci.* **24** (149), 342–353.

VAN ALBADA, G.D., VAN LEER, B. & ROBERTS, JR W.W. 1982 A comparative study of computational methods in cosmic gas dynamics. *Astron. Astrophys.* **108** (1), 76–84.

VREMAN, A.W., SANDHAM, N.D. & LUO, K.H. 1996 Compressible mixing layer growth rate and turbulence characteristics. *J. Fluid Mech.* **320**, 235–258.

WALLIN, S. & JOHANSSON, A.V. 2000 An explicit algebraic Reynolds stress model for incompressible and compressible turbulent flows. *J. Fluid Mech.* **403**, 89–132.

WANG, L. & FU, S. 2011 Development of an intermittency equation for the modeling of the supersonic/hypersonic boundary layer flow transition. *Flow Turbul. Combust.* **87** (1), 165–187.

WILCOX, D.C. 1998 *Turbulence Modeling for CFD*. DCW Industries.

WILCOX, D.C. 2008 Formulation of the k-ω turbulence model revisited. *AIAA J.* **46** (11), 2823–2838.

YAKHOT, V. 2007 Turbulence models generator. arXiv preprint arXiv: 0706.4451.

YAKHOT, V., ORSZAG, S.A., THANGAM, S., GATSKI, T.B. & SPEZIALE, C.G. 1992 Development of turbulence models for shear flows by a double expansion technique. *Phys. Fluids A: Fluid Dyn.* **4** (7), 1510–1520.

YEUNG, P.-K. & POPE, S.B. 1989 Lagrangian statistics from direct numerical simulations of isotropic turbulence. *J. Fluid Mech.* **207**, 531–586.

YOSHIZAWA, A. 1984 Statistical analysis of the deviation of the Reynolds stress from its eddy-viscosity representation. *Phys. Fluids* **27** (6), 1377–1387.

ZHANG, H.Y. 2021 Turbulence modelling for aerodynamic heating in hypersonic flows. *PhD Dissertation*, Department of Mechanical, Aero-space and Civil Engineering, University of Manchester.

ZHANG, H., CRAFT, T. & IACOVIDES, H. 2022 Application of linear and nonlinear two-equation turbulence models in hypersonic flows. *AIAA J.* **60** (6), 3472–3486.

https://doi.org/10.1017/jfm.2025.323 Published online by Cambridge University Press